EUROPEAN RESPIRATORY *journal*

FLAGSHIP SCIENTIFIC JOURNAL OF ERS

Early View

Original article

Targeted Proteomics of Right Heart Adaptation to Pulmonary Arterial Hypertension

Myriam Amsallem, Andrew J. Sweatt, Jennifer Arthur Ataam, Julien Guihaire, Florence Lecerf, Mélanie Lambert, Maria Rosa Ghigna, Md Khadem Ali, Yuqiang Mao, Elie Fadel, Marlene Rabinovitch, Vinicio de Jesus Perez, Edda Spiekerkoetter, Olaf Mercier, Francois Haddad, Roham T. Zamanian

Please cite this article as: Amsallem M, Sweatt AJ, Arthur Ataam J, *et al*. Targeted Proteomics of Right Heart Adaptation to Pulmonary Arterial Hypertension. *Eur Respir J* 2020; in press (https://doi.org/10.1183/13993003.02428-2020).

Targeted Proteomics of Right Heart Adaptation to Pulmonary Arterial Hypertension

Authors: Myriam Amsallem MD PhD[a,b,c]*, Andrew J. Sweatt MD[c,d]*, Jennifer Arthur Ataam PhD[a,b], Julien Guihaire MD PhD[e], Florence Lecerf MS[e], Mélanie Lambert PhD[e], Maria Rosa Ghigna MD PhD[f], Md Khadem Ali PhD[c,d], Yuqiang Mao MD PhD [c,d], Elie Fadel MD PhD[e], Marlene Rabinovitch MD[c,g], Vinicio de Jesus Perez MD[c,d], Edda Spiekerkoetter MD[c,d], Olaf Mercier MD PhD[e], Francois Haddad MD[a,b,c]*, Roham T. Zamanian MD[c,d]*

Affiliations:

[a]Division of Cardiovascular Medicine, Stanford University School of Medicine, Stanford, CA, USA

[b]Cardiovascular Institute, Stanford University School of Medicine, Stanford, CA, USA

[c]Vera Moulton Wall Center at Stanford, Stanford University School of Medicine, Stanford, CA, USA

[d]Division of Pulmonary and Critical Care Medicine, Stanford University School of Medicine, Stanford, CA, USA

[e]Research and Innovation Laboratory, INSERM U999, Marie Lannelongue Hospital, Paris Sud Saclay University, Le Plessis Robinson, France

[f]Division of Pathology, Marie Lannelongue Hospital, Le Plessis Robinson, France

[g]Division of Pediatrics, Stanford University School of Medicine, Stanford, CA, USA

*Both first authors and both senior authors contributed equally.

Please address correspondence to: Myriam Amsallem, MD PhD - Division of Cardiovascular Medicine, Stanford School of Medicine, 300 Pasteur Drive – CA 94305 – Stanford, USA

Take-home message: High plasma HGF levels are associated with right heart maladaptive phenotype and prognostic in PAH. HGF and c-Met RV expression are both increased. Assessing plasma HGF levels might identify patients who warrant closer follow-up and intensified therapy.

Conflict of interest statement: None of the authors have any potential conflicts of interest relative to the study. M.A. has received a 2016 Young Investigator Seed Grant from the Vera Moulton Wall Center at Stanford, a 2019-2020 Stanford Maternal and Child Health Research Institute research seed grant, a research grant from Actelion-Janssen and speaker fees from Bayer. O.M. has been supported by a public grant overseen by the French National Research Agency as part of the second Investissement d'Avenir program (ANR-15-RHUS-0002). E.S. is funded by Stanford Cardiovascular Institute, National Heart Lung Blood Institute (NHLBI) at the National Institute of Health (NIH) R01 HL128734 (E.S. and MK.A.) and Department of Defense grant PR161256 (E.S., Y.M.). F.H. has received research grants from Actelion-Janssen and Philips.

Word count: 3,761

Keywords: Biomarkers; Hepatic Growth Factor; Right Heart Failure; Right Ventricle; Pulmonary Hypertension.

ABSTRACT

No prior proteomic screening study has centered on the right ventricle (RV) in pulmonary arterial hypertension (PAH). This study investigates the circulating proteomic profile associated with right heart maladaptive phenotype (RHMP) in PAH.

Plasma proteomic profiling was performed using multiplex immunoassay in 121 PAH patients (discovery cohort) and 76 patients (validation cohort). The association between proteomic markers and RHMP (defined by the Mayo right heart score [combining RV strain, New York Heart Association NYHA class and NT-proBNP] and Stanford score [RV end-systolic remodeling index, NYHA and NT-proBNP]) was assessed by partial least squares regression. Biomarkers expressions were measured in RV samples from PAH patients and controls, and pulmonary artery banding (PAB) mice.

High levels of hepatic growth factor (HGF), stem cell growth factor beta, nerve growth factor and stromal derived factor-1 were associated with worse Mayo and Stanford scores independently from pulmonary resistance or pressure in both cohorts (the validation cohort had more severe disease features: lower cardiac index and higher NT-proBNP). In both cohorts, HGF added value to the REVEAL score in the prediction of death, transplant, or hospitalization at 3 years. RV expression levels of HGF and its receptor c-Met were higher in end-stage PAH patients than controls, and in PAB mice than shams.

High plasma HGF levels are associated with RHMP and predictive of 3-year clinical worsening. Both HGF and c-Met RV expression levels are increased in PAH. Assessing plasma HGF levels might identify patients at risk for heart failure who warrant closer follow-up and intensified therapy.

ABBREVIATIONS LIST

HGF: hepatic growth factor

MPAP: mean pulmonary arterial pressure

NGF: nerve growth factor

NT-proBNP: N-terminal pro brain natriuretic peptide

NYHA: New York Heart Association

PAB: pulmonary arterial banding

PAH: pulmonary arterial hypertension

PAWP: pulmonary arterial wedge pressure

PH: pulmonary hypertension

REVEAL: registry to evaluate early and long-term PAH disease management

RHF: right heart failure

RV: right ventricle

RVESAI: RV end-systolic area index

RVESRI: RV end-systolic remodeling index

RVFAC: RV fractional area change

RVLS: right ventricular longitudinal strain

TAPSE: tricuspid annular plane systolic excursion

SDF1: stromal derived factor-1

SCGFβ: stem cell growth factor beta

INTRODUCTION

Pulmonary arterial hypertension (PAH) is characterized by progressive obliterative vascular remodeling, which leads to increased right heart afterload. The right ventricle (RV) initially adapts by increasing its wall thickness (adaptive phenotype), but PAH progression often results in RV enlargement and failure (maladaptive phenotype) with subsequent death or lung transplantation [1]. The pathophysiology underlying this transition from an adapted to maladapted RV is not well elucidated, in part because very few PAH research efforts have focused on establishing markers of the right heart maladaptive phenotype (RHMP). Previous proteomic studies of PAH have uncovered blood profiles associated with pulmonary vascular disease severity and outcomes, including our own work, which utilized unsupervised machine learning to identify PAH phenotypes with distinct inflammatory profiles that stratify clinical risk [2, 3]. Emerging evidence suggests a link between inflammation and RV failure in PAH patients and experimental disease models [4, 5], yet no prior proteomic screening study has centered on the right heart.

Recent imaging studies have substantially improved right heart adaptive phenotyping in PAH, identifying RV free-wall longitudinal strain (RVLS) and end-systolic dimensions (such as the remodeling index RVESRI) as strong echocardiographic markers of RV adaptation [6, 7]. These markers have each been integrated with New York Heart Association (NYHA) functional class and N-terminal pro B-type natriuretic peptide (NT-proBNP) to define RHMP scores – a Mayo Clinic model (based on RVLS, NYHA class and NT-proBNP) [6] and a Stanford model (RVESRI, NYHA class and NT-proBNP) [7]. The prognostic value of these simple RV-centered models is equivalent to the REVEAL score [7], a widely adopted PAH risk stratification tool, which requires more extensive clinical data and invasive hemodynamic measures.

Building upon these right heart scores, our primary objective was to identify novel circulating proteomic biomarkers associated with RHMP in PAH. We hypothesized that PAH patients may express a specific blood proteomic profile in association with RHMP, independent of pulmonary disease severity. We also aimed to examine the relationship of these proteomic markers to survival. Finally, we sought to assess tissue-level expression of the RHMP markers in RV samples from end-stage PAH patients and an experimental mouse model of RV pressure overload, to test the hypothesis that increased circulating levels reflect RV overexpression, and to also validate the PAB model for future mechanistic studies.

MATERIAL and METHODS

Study population

This prospective study included group 1 PAH patients enrolled into the Stanford University Pulmonary Hypertension Biobank (Stanford, CA) between 2008 and 2014, who had plasma collected for proteomic profiling within two weeks of a routine echocardiogram (**Figure 1**, **Supplementary Methods**). PAH diagnosis required mean pulmonary arterial pressure (MPAP) ≥25 mmHg, pulmonary arterial wedge pressure ≤15 mmHg, and pulmonary vascular resistance (PVR) >240 dyn.s.cm^{-5}. Exclusion criteria were chronic infection (n=7), primary immunodeficiency (n=1), recent acute illness other than heart failure (within 1 month) (n=8), congenital systemic-to-pulmonary shunt (n=10), active malignancy (n=4), missing echocardiogram within 2 weeks (n=68), or suboptimal echocardiographic data (n=6). Study baseline was the date of blood collection. Patients were divided into a discovery (n=121, 2008-2011) and validation cohort (n=76, 2012-2014). Plasma was also obtained from healthy controls (n=88), who underwent rigorous screening to establish

health. Stanford Institutional Review Board approved the study (IRB #14083 and #20942); all subjects provided written informed consent.

Blood proteomic profiling

Fasting blood samples were collected from an antecubital vein, processed to plasma, and stored according to protocols (**Supplementary Methods**). A targeted proteomic panel of 48 cytokines, chemokines and growth factors (**Table 1** and **Table E1**) was measured for each subject using Bio-Plex multiplex immunoassay (BioRad Inc., Hercules, CA), a bead-based flow cytometric platform built on Luminex® xMAP ™ technology (Luminex Corp., Austin, TX), according to manufacturer instructions (**Supplementary Methods**). Each sample was measured in duplicate. A Luminex 200 plate reader quantified median fluorescence intensity (MFI) for each protein. MFI was used for all analyses rather than standard curve-derived absolute concentrations, as MFI does not require detection limit censoring and has better downstream statistical power [8]. The inter-assay coefficient of variation was <15% for all measured analytes, based on internal controls included across runs.

Clinical data collection

Transthoracic echocardiogram studies were acquired using Philips IE 33 ultrasound systems (Philips, Amsterdam, Netherlands). RV dimensions and functional metrics were measured on RV-focused apical 4-chamber views, averaged over three cycles, and included RVESRI (defined by the lateral wall to septal height ratio) and RVLS as previously published (**Supplementary Methods**) [7]. These measurements were used to calculate two right heart adaptive phenotyping scores, the Mayo Clinic score integrating RVLS, NYHA class and NT-proBNP, and the Stanford score integrating RVESRI, NYHA class and NT-proBNP (**Table E2**). Follow-up echocardiograms available in survivors at 1 year were interpreted using the same methodology.

Right heart remodeling with therapy was defined by changes in RVESRI from baseline (improvement if relative delta <10%, worsening if >10% and stable otherwise) as previously published [7].

NYHA class, six-minute walk distance, diffusing capacity of the lung for carbon monoxide, MDRD estimated glomerular filtration rate and NT-proBNP levels were collected if available within 1 month of baseline. Hemodynamic data (right atrial pressure, MPAP, pulmonary arterial wedge pressure, PVR, and cardiac index) were obtained when right heart catheterization was performed within 3 months of inclusion. Data were used to calculate the REVEAL risk score (**Table E3**) [9].

Patients were prospectively followed to evaluate the primary endpoint of clinical worsening (i.e. death, lung transplantation, or hospitalization for acute right heart failure), and the secondary end point (death or lung transplant).

Pathology analysis of human RV samples

RV frozen and paraffin-embedded biopsies of explanted hearts were obtained from 4 PAH patients (**Table E4**) who underwent heart-lung transplant at Marie Lannelongue Hospital (IRB #18.06.06, Le Plessis-Robinson, France). For comparison, we acquired RV frozen biopsies from 5 control heart donors (without cardiovascular disease or PH) whose organs were not transplanted (paraffin-embedded biopsies were not available); Explanted hearts were procured from the INSERM URMS 1148 biobank (BRIF BB-0033-00029, BBMRI-EU/infrastructure), approved by the French National Ethics Committee (N°: PFS17-002) and declared at the French Ministry of Research (DC-2018-3141).

Upon identifying RHMP circulating biomarkers in the clinical cohorts, we (i) compared tissue-level expression of these proteins and their receptors in PAH and controls by incubating

frozen RV samples with primary specific antibodies (Abcam, Cambridge, UK) and performing western blots, and (ii) localized the RHMP biomarkers in RV tissue from PAH patients with immunofluorescence staining and confocal microscopy (Zeiss LSM 800 microscope with ZEN software; Carl Zeiss Microscopy, White Plains, NY) (**Supplementary Methods**).

Pulmonary Artery Banding (PAB) mouse model RV analysis

All animal experiments were performed in accordance with National Research Council guidelines (*Guide for Care and Use of Laboratory Animals*) and approved by local authorities (APLAC, Stanford University, Protocol #27626). Chronic RV pressure overload was induced in 10-14 week-old male C57BL/6 mice as previously published [10] and detailed in **Supplementary Methods.** Anesthetized animals underwent thoracotomy, 6-0 silk sutures were used to band the main pulmonary artery (PA), and one-week post-surgery a peak pressure gradient >15 mmHg was confirmed across the band by echocardiography (GE Vivid 7). A control group of age-matched littermates underwent sham surgery (PA isolation without suture placement). MPAP, heart rate, and pulmonary valve velocity time integral were measured by echocardiography after 5 weeks to document reduced cardiac output and RV samples were collected and snap frozen. After isolating RNA from homogenized RV samples, we applied quantitative reverse transcriptase-PCR (Applied Biosystems, Foster City, CA) to measure expression levels of the mRNA transcripts corresponding to RHMP proteomic markers of interest.

Statistical analysis

Baseline characteristics were compared using Student's t-test or Mann-Whitney-Wilcoxon test for continuous data, and Chi-square test for categorical data. Proteomic data preprocessing involved background fluorescence subtraction, plate/batch adjustment (empirical Bayes

methodology) [11], robust quantile normalization, duplicate averaging, and adjustment for age, sex and body mass index. To identify RHMP markers, partial least squares (PLS) regression models were fit using the 'SIMPLS' algorithm (**Supplementary Methods**). RHMP markers were selected by assessing (i) variable importance for projections (VIP) scores and (ii) regression beta coefficients (using t-tests of coefficients based on variance estimates from jack-knife resampling). PLS models were fit to associate proteins with Mayo and Stanford scores, individual components of each score, and pulmonary hemodynamics. RHMP biomarkers were identified as the common biomarkers associated with RHMP in both cohorts. Levels of the identified RHMP biomarkers were examined among low, intermediate, and high-risk RV phenotypes (based on Mayo and Stanford scores) to compare each risk group to controls (Kruskal-Wallis and post-hoc Dunn tests) and confirm a trend across ordered PAH groups (Cuzick test). To relate biomarkers to outcomes, Kaplan-Meier estimates of transplant- and hospitalization-free survival were compared across quartiles by log-rank statistics, and Cox proportional hazards regression models were fit. Circulating biomarkers were added as continuous variables. Scaled Schoenfeld residuals were plotted against time for each variable, to ensure the proportional hazards assumption was met. Hazard ratios were normalized to the standard deviation of predictor variables. To determine whether each biomarker added incremental value to established risk scores for prediction of 3-year outcome, $\chi 2$ values were compared. Binary logistic regression model was used to determine whether biomarkers or right heart metrics were predictive of RVESRI improvement (relative delta <10%) at 1 year. Patients included in 2014 with <3 years follow-up (n=4) were right censored. Statistical analyses were performed using SPSS® v.19 (SPSS Inc, Chicago, IL) and R v.3.5.1 (R Core Team, Vienna, Austria) software programs.

RESULTS

Proteomic profiling of RHMP in patients with PAH

Table 2 summarized baseline characteristics of the discovery cohort. High levels of hepatic growth factor (HGF), stem cell growth factor (SCGFβ or CLEC11A), nerve growth factor (NGF) and stromal cell-derived factor 1 (SDF1 or CXCL12) were more strongly associated with higher-risk Mayo and Stanford scores, RV dysfunction (RVLS), RV adverse remodeling (RVESRI), higher NT-proBNP and worse NYHA functional class than with pulmonary disease severity (**Figure 2A, Table E5** and **Figure E1)**.

The validation cohort had more severe pulmonary disease features, fewer patients on background therapy and a higher frequency of incident cases than the discovery cohort (**Table 2**). REVEAL, Mayo and Stanford risk scores distributions were similar in the two cohorts. High levels of HGF, SCGFβ, NGF, and to a lesser extent SDF1, were associated with higher-risk Mayo and Stanford scores, RV dysfunction, higher NT-proBNP and worse NYHA functional class (**Figure 2A**). No measured cytokine was found to have a positive association with favorable right heart metrics across both cohorts.

Figure 2B-C compared the 4 candidate RHMP markers levels in both cohorts combined among low, intermediate, and high-risk RV patient subgroups, and the 88 healthy controls (median age 58 [44-64] years, 52.3% were female). Circulating levels of the 4 markers did not differ according to gender in patients or in controls (**Figure E2**). HGF and NGF levels did not significantly differ according to ethnicity and race among patients with PAH (**Figure E2**), while non-Hispanic White patients had lower levels of SCGFβ than Hispanic patients ($p<0.01$) and lower SDF1a levels than Hispanic and Asian patients ($p=0.04$).

Prognostic value of HGF

During a median follow-up of 3.14 [2.16; 5.44] years, the primary end point was reached in 76 patients (58 were hospitalized, 10 transplanted and overall 41 died). Event-free survival rates (± standard error) for the primary end point were 91 ±2% at 1 year, 78 ±3% at 3 years, and 62 ±34% at 5 years (**Figure 3A**). The secondary end point of death or transplant was reached in 49 patients.

Using univariable analysis, HGF and SCGFβ were associated with the primary end point (HR=1.54 [1.24; 1.91], p<0.0001 and 1.26 [1.12; 1.59], p=0.02 respectively), while NGF (p=0.83) and SDF1a (p=0.89) were not. Kaplan–Meier survival curves for the primary end point according to HGF (p<0.001) and SCGFβ quartiles (p=0.002) are presented in **Figure 3B** and **Figure E3**. HGF added significant incremental value to the Mayo, Stanford and REVEAL scores for prediction of the primary end point at 3 years (p<0.05, **Figure 3C** and **Table E6**). Both HGF and SCGFβ were also associated with the secondary end point of death or transplant (HR=1.71 [1.38; 2.12], p<0.0001, and 1.26 [1.01; 1.59], p=0.02 respectively).

Absence of biomarker of longitudinal cardiac remodeling

Among the total population, 174 patients (93.0% of 1-year survivors) had a follow-up echocardiogram at 1 year (median time to follow-up study was 1.03 [0.85; 1.35] years). Parenteral prostanoids were initiated in 37 patients between baseline and follow-up, while PH-specific therapies were not changed in 55 patients. None of the 4 RHMP biomarkers at baseline (entered as continuous variables using binary regression analyses) were found to be significantly associated with changes in right heart remodeling, irrespective of the therapy initiated between baseline and the follow-up echocardiogram. Similarly, the Stanford score (p=0.50), Mayo score

(p=0.99) and NT-proBNP (p=0.06, OR=1.85 [0.98; 3.49]) at baseline were not associated with changes in right heart remodeling at follow-up.

Human RV tissue-level expression of RHMP biomarkers

Protein levels of HGF and its receptor c-Met were higher in RV specimens from PAH patients than controls (**Figure 4**). The levels of NGF were decreased and its receptor tropomyosin-related receptor kinase A (TrkA) increased in PAH as compared to controls. In patients with PAH, RV fibrosis level assessed by the % area of Picro-Sirius Red staining was 11.5 [8.8- 15.7]%, similar across PAH etiology (**Figure E4** and **Supplementary Methods**). **Figure 5** and **Figure E5** show the localization of the 4 biomarkers and receptors in RV samples from the patient with idiopathic PAH. Both PAH patients (idiopathic and BMPR2 mutation) exhibited qualitatively similar protein RV expression. The receptor c-Met colocalized with cardiomyocytes, smooth muscle cells, endothelial cells and fibroblasts markers, and to a lesser extent with macrophages (**Figure 5**). Punctiform expression of HGF was observed in a vesicle pattern, more abundantly in cardiomyocytes, smooth muscle cells, and to a lesser extent in macrophages and fibroblasts. Both TrkA and NGF colocalized with cardiomyocytes, smooth muscle cells and macrophages, while TrkA additionally colocalized with fibroblasts and NGF with endothelial cells (**Figure E5**). SCGFβ was present in cardiomyocytes, smooth muscle cells and fibroblasts, and SDF1 was found in cardiomyocytes, smooth muscle cells, endothelial cells and macrophages.

Altered RV expression of growth factors *Hgf, c-Met, Ngf and Scgfβ* in PAB mice

Five weeks after PAB or sham surgery, the RNA expression of *Hgf, c-Met and Ngf* were significantly increased (all $p<0.01$) whereas the expression of *Scgfβ* was significantly decreased ($p<0.001$) in RV homogenates from PAB compared to shams, as presented in **Figure E6**.

DISCUSSION

This targeted proteomics study identifies four circulating cytokines associated with RHMP, independently from pulmonary hemodynamic severity. HGF emerges as a strong predictor of clinical worsening at 3 years, incremental to the REVEAL score. The protein expression of c-Met and HGF is increased in the RV of deceased PAH patients in cardiomyocytes, smooth muscle cells and endothelial cells. The PAB mouse model further confirms increased RV gene expression of *Hgf* and *c-Met*, suggesting PAB to be a valid model to further mechanistically study the involvement of this pathway in RV adaptation to pulmonary hypertension (PH) over time, and answer the question of whether increasing HGF expression represents a beneficial or deleterious response; information potentially useful from a therapeutic aspect. The study originality resides in its design (going from supervised bedside -omics screening to the target organ and bench analysis), which is a novel approach to the pressure-overloaded right heart. This approach has allowed us to use the blood as a window to right heart failure in PAH, leading to the identification of HGF/c-Met as a potential signaling pathway of interest.

HGF is a mesenchymal-derived pleiotropic cytokine binding to its tyrosine kinase receptor c-Met [12]. The HGF/c-Met signaling pathway promotes angiogenesis and cardiomyocytes survival, inhibits fibrosis in experimental myocardial infarction and left cardiomyopathy models [13, 14] and inhibits vascular permeability and inflammation [15, 16]. Despite the cardioprotective effects of HGF on the left heart, several studies have paradoxically reported the association between high circulating levels of HGF and left ventricular remodeling, dysfunction or adverse outcomes in several pressure-overloaded cardiac diseases (hypertension and aortic stenosis), or advanced ischemic left heart failure [17–19].

Evidence on the molecular role of HGF/c-Met in the right heart is sparse. High levels of HGF have been reported in small cohorts of patients with scleroderma-associated [20] or idiopathic PAH in whom HGF correlated with MPAP [21]. In another study conducted in patients with idiopathic, familial or associated PAH, HGF levels did not correlate with any clinical markers of disease severity [22]. Our study further demonstrates the association of high plasma HGF levels with RHMP beyond pulmonary disease severity. Including two cohorts differing in terms of demographics, prevalence/incidence repartition, and functional severity strengthens the results, suggesting that the biomarkers identified are associated with RV adaptation across PAH etiology. High HGF levels were strongly associated with outcome in our cohort, adding incremental value to the REVEAL risk score, suggesting the timely role of the HGF/c-Met axis on the right heart. None of the 4 RHMP biomarkers but also none of the right heart scores or NT-proBNP levels (validated prognostic markers) at baseline were associated with right heart remodeling improvement at 1 year, irrespective of the therapy initiated, illustrating the distinction between prognostic markers and markers predictive of response to therapy. Future studies should investigate whether changes in biomarkers levels from baseline to 1 year would correlate with changes in right heart remodeling.

The origin of increased HGF plasma levels in PAH remains to be fully elucidated, either resulting from increased production of HGF and/or alterations in its systemic clearance. Increased expression of HGF, SDF1a and other myeloid-activating factors by primary endothelial cells harvested from human PAH lungs under hypoxic conditions have been previously reported [22]. A cardiac contribution of high circulating HGF levels, in the context of damaged myocardium, cannot be excluded. In the present study, we report the increased protein expression of HGF and c-Met in the RV of patients with PAH with end-stage right heart failure

requiring a heart-lung transplant, across PAH etiology. Another original finding is the localization of these markers in the RV of patients with PAH, suggesting the pleiotropic effect of HGF/c-Met as previously demonstrated in the left ventricle [12]. The other markers did not show this increased expression in RV samples from patients with PAH as compared to controls, although limited by the number of samples available, which warrants further investigation.

Animal models bring some insights into the potential origin of circulating HGF levels. Increased HGF plasma levels at 2 weeks have been reported in rats with monocrotaline-induced PH, associated with increase in RV mRNA expression of *Hgf* and *c-Met* at 4 weeks, but not in the liver, suggesting a cardiac rather than hepatic origin of plasma HGF [23]. Our PAB model [10] further demonstrates the increased gene expression of *Hgf* and *c-Met* in RV homogenates from PAB compared to shams (adding to the evidence of increased protein expression in our human samples), suggesting that increased circulating levels of HGF in peripheral blood and in the right ventricles of patients with PAH could reflect an increased HGF production in the RV. These data though do not allow the conclusion as to whether increased HGF production in the RV reflects a compensatory attempt of the RV to adapt to an increased afterload or whether it represents rather a harmful response of maladaptation, and further studies using the PAB model will be of high value to clarify the timing and role of the HGF-Met pathways in the pressure-overloaded RV.

The potential beneficial role of HGF as a therapy in PAH has been previously discussed [24]. HGF increases expression of the Bone Morphogenetic Protein Receptor 2 (BMPR2) [25], a pathway mutated in the familial form of PAH, downregulated in non-genetic forms and associated with impaired RV hypertrophy and contractility in small animal models of PH [26, 27]. The activation of BMPR2 is of benefit to PAH and associated RV failure [28], therefore the

effects of HGF on BMPR2 could constitute a potential therapy targeting the right heart in PAH. Several animal models (e.g. rats with monocrotaline-induced PH, rabbits with shunt flow-induced PH) have shown that exogenous HGF or *Hgf* gene transfection reduced the development of PH, which was associated with less marked right heart hypertrophy and lower inflammatory profiles than shams [29–32]. However, the timely and direct effect of the HGF/c-Met axis activation in the right heart remains to be elucidated. Here the PAB model might be of particular value to explore the dynamic changes in plasma and tissue HGF expression over time and potential reversibility with de-banding [10].

NGF promotes cardiomyocyte survival and is the main neurotrophic factor increasing cardiac sympathetic activity [33, 34]. Higher secretion and endothelial expression of NGF from pulmonary arteries of patients with PH secondary to chronic obstructive pulmonary disease than controls without PH have been reported [35]. However, there was no significant increase in the secretion or lung expression of NGF in patients with idiopathic PAH in this study. NGF was further shown to induce hyperreactivity to vasoconstrictors in rat and human isolated pulmonary arteries, proliferation and migration of human pulmonary arterial smooth muscle cells and endothelial cells, and secretion of the proinflammatory cytokines IL-1β and TNF-α [35]. Anti-NGF blocking antibodies reversed PH in the PH animal models, decreasing pulmonary vascular remodeling, hyperreactivity and inflammation [35]. Another study in rats with RV hypertrophy secondary to monocrotaline-induced PH reported the upregulation of NGF associated with deterioration of neuronal cellular function [36]. In humans, NGF has been shown to be downregulated in patients with end-stage left heart failure [37, 38], consistent with our immunoblot findings, suggesting a time-variability of this factor in heart failure.

Higher plasmatic concentrations of SCGFβ have been documented in patients with idiopathic and scleroderma-associated PAH as compared to scleroderma patients without PAH [39]. High circulating SCGFβ levels have been reported in patients with dilated cardiomyopathy and Chagas disease, without association with outcomes [40]. Finally, increased plasmatic levels of SDF1a, involved in pulmonary artery muscularization in PAH [41], have been reported in 61 patients with idiopathic PAH as compared to healthy controls; SDF1a levels also correlated with NT-proBNP and RV function [4].

Study limitations

The first limitation derives from its single-center design. The fact that the two cohorts were collected and analyzed at two different time points, excluding the risk of batch effect in the proteomics analysis, contributes to increasing the confidence in the results. The second limitation derives from the cross-sectional nature of the biomarker analyses, which were only available at baseline. Further studies are needed to investigate whether longitudinal changes in circulating biomarkers would be prognostic or predictive of response to therapy in patients with PAH. The third limitation comes from the absence of RV paraffin-embedded biopsies from controls, which precluded us from assessing whether the increase in HGF protein expression in PAH is observed in all cell types or is specific for a cell type.

In conclusion, high plasma levels of HGF are associated with right heart maladaptive phenotype in PAH and are incremental to the REVEAL score for prediction of outcomes. As both RV HGF-cMet protein and gene expression are increased in PAH, this pathway warrants further exploration as a potential RV-specific therapeutic target. Assessing plasma HGF levels

might identify PAH patients at risk for right heart failure and outcomes who warrant closer follow-up and intensified PAH therapy.

ACKNOWLEDGMENTS

The authors would like to thank Andrew Hsi (Stanford University, CA, USA) for Stanford database management, Lilia Lamrani, MS (Marie Lannelongue Hospital - Paris Sud Paris Saclay University, France) for her help with clinical data collection and Jean-Baptiste Michel, MD, PhD (Paris VII University, France) for facilitating the procurement of controls cardiac biopsies. The authors would like to address a special thought to late Catherine Rucker-Martin PhD (from Marie Lannelongue Hospital - Paris Sud Paris Saclay University, France) who contributed to the immunofluorescence experiments and study design. The authors would like to thank the Vera Moulton Wall Center of Pulmonary Hypertension at Stanford and the Stanford Cardiovascular Institute for their funding support.

REFERENCES

1. Vonk Noordegraaf A, Westerhof BE, Westerhof N. The Relationship Between the Right Ventricle and its Load in Pulmonary Hypertension. J Am Coll Cardiol 2017; 69: 236–243.

2. Rhodes CJ, Wharton J, Ghataorhe P, Watson G, Girerd B, Howard LS, Gibbs JSR, Condliffe R, Elliot CA, Kiely DG, Simonneau G, Montani D, Sitbon O, Gall H, Schermuly RT, Ghofrani HA, Lawrie A, Humbert M, Wilkins MR. Plasma proteome analysis in patients with pulmonary arterial hypertension: an observational cohort study. Lancet Respir Med 2017; 5: 717–726.

3. Sweatt AJ, Hedlin HK, Balasubramanian V, Hsi A, Blum LK, Robinson WH, Haddad F, Hickey PM, Condliffe R, Lawrie A, Nicolls MR, Rabinovitch M, Khatri P, Zamanian RT. Discovery of Distinct Immune Phenotypes Using Machine Learning in Pulmonary Arterial Hypertension. Circ Res 2019; 124: 904–919.

4. Yang T, Li Z-N, Chen G, Gu Q, Ni X-H, Zhao Z-H, Ye J, Meng X-M, Liu Z-H, Xiong C-M, He J-G. Increased levels of plasma CXC-Chemokine Ligand 10, 12 and 16 are associated with right ventricular function in patients with idiopathic pulmonary arterial hypertension. Heart Lung J Crit Care 2014; 43: 322–327.

5. Sydykov A, Mamazhakypov A, Petrovic A, Kosanovic D, Sarybaev AS, Weissmann N, Ghofrani HA, Schermuly RT. Inflammatory Mediators Drive Adverse Right Ventricular Remodeling and Dysfunction and Serve as Potential Biomarkers. Front Physiol 2018; 9: 609.

6. Fine NM, Chen L, Bastiansen PM, Frantz RP, Pellikka PA, Oh JK, Kane GC. Outcome prediction by quantitative right ventricular function assessment in 575 subjects evaluated for pulmonary hypertension. Circ Cardiovasc Imaging 2013; 6: 711–721.

7. Amsallem M, Sweatt AJ, Aymami MC, Kuznetsova T, Selej M, Lu H, Mercier O, Fadel E, Schnittger I, McConnell MV, Rabinovitch M, Zamanian RT, Haddad F. Right Heart End-Systolic Remodeling Index Strongly Predicts Outcomes in Pulmonary Arterial Hypertension: Comparison With Validated Models. Circ Cardiovasc Imaging 2017; 10:e005771.

8. Breen EJ, Tan W, Khan A. The Statistical Value of Raw Fluorescence Signal in Luminex xMAP Based Multiplex Immunoassays. Sci Rep 2016; 6: 26996.

9. Benza RL, Miller DP, Gomberg-Maitland M, Frantz RP, Foreman AJ, Coffey CS, Frost A, Barst RJ, Badesch DB, Elliott CG, Liou TG, McGoon MD. Predicting survival in pulmonary arterial hypertension: insights from the Registry to Evaluate Early and Long-Term Pulmonary Arterial Hypertension Disease Management (REVEAL). Circulation 2010; 122: 164–172.

10. Boehm M, Tian X, Mao Y, Ichimura K, Dufva MJ, Ali K, Prosseda SD, Shi Y, Kuramoto K, Reddy S, Kheyfets VO, Metzger RJ, Spiekerkoetter E. Delineating the molecular and histological events that govern right ventricular recovery using a novel mouse model of PA de-banding. Cardiovasc Res 2019;;cvz310.

11. Johnson WE, Li C, Rabinovic A. Adjusting batch effects in microarray expression data using empirical Bayes methods. Biostat 2007; 8: 118–127.

12. Gallo S, Sala V, Gatti S, Crepaldi T. HGF/Met Axis in Heart Function and Cardioprotection. Biomedicines 2014; 2: 247–262.

13. Aoki M, Morishita R, Taniyama Y, Kida I, Moriguchi A, Matsumoto K, Nakamura T, Kaneda Y, Higaki J, Ogihara T. Angiogenesis induced by hepatocyte growth factor in non-infarcted myocardium and infarcted myocardium: up-regulation of essential transcription factor for angiogenesis, ets. Gene Ther 2000; 7: 417–427.

14. Nakamura T, Mizuno S, Matsumoto K, Sawa Y, Matsuda H, Nakamura T. Myocardial protection from ischemia/reperfusion injury by endogenous and exogenous HGF. J Clin Invest 2000; 106: 1511–1519.

15. Mizuno S, Nakamura T. Prevention of neutrophil extravasation by hepatocyte growth factor leads to attenuations of tubular apoptosis and renal dysfunction in mouse ischemic kidneys. Am J Pathol 2005; 166: 1895–1905.

16. Rutella S, Bonanno G, Procoli A, Mariotti A, de Ritis DG, Curti A, Danese S, Pessina G, Pandolfi S, Natoni F, Di Febo A, Scambia G, Manfredini R, Salati S, Ferrari S, Pierelli L, Leone G, Lemoli RM. Hepatocyte growth factor favors monocyte differentiation into regulatory interleukin (IL)-10++IL-12low/neg accessory cells with dendritic-cell features. Blood 2006; 108: 218–227.

17. Rychli K, Richter B, Hohensinner PJ, Kariem Mahdy A, Neuhold S, Zorn G, Berger R, Mörtl D, Huber K, Pacher R, Wojta J, Niessner A, Hülsmann M. Hepatocyte growth factor is a strong predictor of mortality in patients with advanced heart failure. Heart 2011; 97: 1158–1163.

18. Kuznetsova T, Haddad F, Knez J, Rosenberg-Hasson Y, Sung J, Cauwenberghs N, Thijs L, Karakikes I, Maecker H, Mahaffey KW, Wu JC, Staessen JA. Cytokines profile in hypertensive patients with left ventricular remodeling and dysfunction. J Am Soc Hypertens 2015; 9: 975-984.e3.

19. Kim JB, Kobayashi Y, Kuznetsova T, Moneghetti KJ, Brenner DA, O'Malley R, Dao C, Wu JC, Fischbein M, Craig Miller D, Yeung AC, Liang D, Haddad F, Fearon WF. Cytokines profile of reverse cardiac remodeling following transcatheter aortic valve replacement. Int J Cardiol 2018; 270: 83–88.

20. Riccieri V, Stefanantoni K, Vasile M, Macrì V, Sciarra I, Iannace N, Alessandri C, Valesini G. Abnormal plasma levels of different angiogenic molecules are associated with different clinical manifestations in patients with systemic sclerosis. Clin Exp Rheumatol 2011; 29: S46-52.

21. Liang M, Pang Y, Zhang S, Zhang M. Utility of Hepatocyte Growth Factor as a Biomarker for Early Diagnosis of Pulmonary Artery Hypertension. Mol Diagn Ther 2016; 20: 463–468.

22. Farha S, Asosingh K, Xu W, Sharp J, George D, Comhair S, Park M, Tang WHW, Loyd JE, Theil K, Tubbs R, Hsi E, Lichtin A, Erzurum SC. Hypoxia-inducible factors in human pulmonary arterial hypertension: a link to the intrinsic myeloid abnormalities. Blood 2011; 117: 3485–3493.

23. Radik M, Kmecova Z, Veteskova J, Malikova E, Doka G, Krenek P, Klimas J. Hepatocyte growth factor plays a particular role in progression of overall cardiac damage in experimental pulmonary hypertension. Int J Med Sci 2019; 16: 854–863.

24. Guo Y-H, Su L-X, Guo N, Liu C-T. Novel therapy for idiopathic pulmonary arterial hypertension: Can hepatocyte growth factor be beneficial? J Geriatr Cardiol 2012; 9: 211–212.

25. Ye L, Lewis-Russell JM, Davies G, Sanders AJ, Kynaston H, Jiang WG. Hepatocyte growth factor up-regulates the expression of the bone morphogenetic protein (BMP) receptors, BMPR-IB and BMPR-II, in human prostate cancer cells. Int J Oncol 2007; 30: 521–529.

26. Hemnes AR, Brittain EL, Trammell AW, Fessel JP, Austin ED, Penner N, Maynard KB, Gleaves L, Talati M, Absi T, Disalvo T, West J. Evidence for right ventricular lipotoxicity in heritable pulmonary arterial hypertension. Am J Respir Crit Care Med 2014; 189: 325–334.

27. Hautefort A, Mendes-Ferreira P, Sabourin J, Manaud G, Bertero T, Rucker-Martin C, Riou M, Adão R, Manoury B, Lambert M, Boet A, Lecerf F, Domergue V, Brás-Silva C, Gomez AM, Montani D, Girerd B, Humbert M, Antigny F, Perros F. Bmpr2 Mutant Rats Develop Pulmonary and Cardiac Characteristics of Pulmonary Arterial Hypertension. Circulation 2019; 139: 932–948.

28. Spiekerkoetter E, Tian X, Cai J, Hopper RK, Sudheendra D, Li CG, El-Bizri N, Sawada H, Haghighat R, Chan R, Haghighat L, de Jesus Perez V, Wang L, Reddy S, Zhao M, Bernstein D, Solow-Cordero DE, Beachy PA, Wandless TJ, Ten Dijke P, Rabinovitch M.

FK506 activates BMPR2, rescues endothelial dysfunction, and reverses pulmonary hypertension. J Clin Invest 2013; 123: 3600–3613.

29. Ono M, Sawa Y, Mizuno S, Fukushima N, Ichikawa H, Bessho K, Nakamura T, Matsuda H. Hepatocyte growth factor suppresses vascular medial hyperplasia and matrix accumulation in advanced pulmonary hypertension of rats. Circulation 2004; 110: 2896–2902.

30. Ono M, Sawa Y, Fukushima N, Suhara H, Nakamura T, Yokoyama C, Tanabe T, Matsuda H. Gene transfer of hepatocyte growth factor with prostacyclin synthase in severe pulmonary hypertension of rats. Eur J Cardio-Thorac Surg 2004; 26: 1092–1097.

31. Wang W, Liu K, Zhang F, Cao G, Zhang Y, Liu R, Wu S. Recombinant human hepatocyte growth factor transfection alleviates hyperkinetic pulmonary artery hypertension in rabbit models. J Thorac Cardiovasc Surg 2013; 146: 198–205.

32. Chen J, Zhang H, Zhang R, Liu Z, Wang J, Xiao M, Ba M, Yao F, Liu J, Huang S, Zhong J. Transfer of human hepatocyte growth factor reduces inflammation and prevents pulmonary arterial remodeling in monocrotaline-induced. Int J Clin Exp Pathol 2014; 7: 8763–8769.

33. Hassankhani A, Steinhelper ME, Soonpaa MH, Katz EB, Taylor DA, Andrade-Rozental A, Factor SM, Steinberg JJ, Field LJ, Federoff HJ. Overexpression of NGF within the heart of transgenic mice causes hyperinnervation, cardiac enlargement, and hyperplasia of ectopic cells. Dev Biol 1995; 169: 309–321.

34. Caporali A, Sala-Newby GB, Meloni M, Graiani G, Pani E, Cristofaro B, Newby AC, Madeddu P, Emanueli C. Identification of the prosurvival activity of nerve growth factor on cardiac myocytes. Cell Death Differ 2008; 15: 299–311.

35. Freund-Michel V, Cardoso Dos Santos M, Guignabert C, Montani D, Phan C, Coste F, Tu L, Dubois M, Girerd B, Courtois A, Humbert M, Savineau J-P, Marthan R, Muller B. Role of Nerve Growth Factor in Development and Persistence of Experimental Pulmonary Hypertension. Am J Respir Crit Care Med 2015; 192: 342–355.

36. Kimura K, Ieda M, Kanazawa H, Yagi T, Tsunoda M, Ninomiya S, Kurosawa H, Yoshimi K, Mochizuki H, Yamazaki K, Ogawa S, Fukuda K. Cardiac sympathetic rejuvenation: a link between nerve function and cardiac hypertrophy. Circ Res 2007; 100: 1755–1764.

37. Kaye DM, Vaddadi G, Gruskin SL, Du XJ, Esler MD. Reduced myocardial nerve growth factor expression in human and experimental heart failure. Circ Res 2000; 86: E80-84.

38. Qin F, Vulapalli RS, Stevens SY, Liang C-S. Loss of cardiac sympathetic neurotransmitters in heart failure and NE infusion is associated with reduced NGF. Am J Physiol Heart Circ Physiol 2002; 282: H363-371.

39. Stefanantoni K, Sciarra I, Vasile M, Badagliacca R, Poscia R, Pendolino M, Alessandri C, Vizza CD, Valesini G, Riccieri V. Elevated serum levels of macrophage migration inhibitory factor and stem cell growth factor β in patients with idiopathic and systemic sclerosis associated pulmonary arterial hypertension. Reumatismo 2015; 66: 270–276.

40. Wang Y, Khan A, Heringer-Walther S, Schultheiss H-P, Moreira M da CV, Walther T. Prognostic value of circulating levels of stem cell growth factor beta (SCGF beta) in patients with Chagas' disease and idiopathic dilated cardiomyopathy. Cytokine 2013; 61: 728–731.

41. Yuan K, Liu Y, Zhang Y, Nathan A, Tian W, Yu J, Sweatt AJ, Shamshou EA, Condon D, Chakraborty A, Agarwal S, Auer N, Zhang S, Wu JC, Zamanian RT, Nicolls MR, de Jesus Perez VA. Mural Cell SDF1 Signaling Is Associated with the Pathogenesis of Pulmonary Arterial Hypertension. Am J Respir Cell Mol Biol 2020; 62: 747–759.

FIGURE LEGENDS

Figure 1. Study design. PAB: pulmonary arterial banding; PAH: pulmonary artery hypertension; RHMP: right heart maladaptive phenotype.

Figure 2. (a) Variable Importance in Projection (VIP) scores and correlations for each cytokine with respect to right heart scores and metrics in both cohorts and (b) Levels of the 4 markers according to levels of right heart maladaptive phenotype in patients with pulmonary arterial hypertension (PAH) and controls. (a) Using partial least square regression, we assessed the correlations between plasma proteomic markers (using multiplex immunoassay) and markers of right heart maladaptive phenotype (Stanford right heart RH score based on RVESRI, NYHA class and NT-proBNP levels; Mayo RH score based on RVLS, NYHA class and NT-proBNP levels; RVESRI; RVLS; NT-proBNP; NYHA FC; mPAP and PVR) in 121 PAH patients (discovery cohort from 2008-2011) and 76 (validation cohort from 2012-2014). Positive correlations are shown in red, negative in blue. **(b)** Analyte levels of the 4 strongest biomarkers associated with right heart maladaptive phenotype according to tertiles of the Stanford RH score (upper panel) or Mayo RH score (lower panel) in patients with PAH and in the 88 healthy controls. Comparison between each right heart risk category to controls was performed using Dunn's Kruskal Wallis test (across-groups among patients with PAH) with post-hoc pairwise comparisons adjusted for multiple testing (Benjamini Hochberg). The p values of the Cuzick test was used to confirm an increasing trend of cytokine levels across ordered categories (from low to intermediate to high). MPAP: mean pulmonary arterial hypertension; NYHA FC: New York Heart Association functional class; PVR: pulmonary vascular resistance;

RH: right heart; RVLS: right ventricular free-wall longitudinal strain is presented in absolute value (lowest values indicate worst right ventricular dysfunction); RVESRI: right ventricular end-systolic remodeling index. For cytokines abbreviations, please see **Table 1** and supplementary **Table S1**.

Figure 3. Prognostic value of hepatic growth factor (HGF) and its incremental value to risk scores for outcome prediction. (a) Five-year Kaplan Meier survival curves for the primary combined end point of death, lung transplant or hospitalization for acute right heart failure of the total PAH cohort (n=197) and **(b)** according to quartiles of hepatic growth factor levels at baseline. **(c)** $\chi 2$ of scores and HGF, nerve growth factor (NGF), stem cell growth factor beta (SCGFβ) and stromal cell-derived factor 1 (SDF1) for prediction of the primary end point (death, transplant, or admission for right heart failure) at 3 years in the total PAH cohort (n=197) using Cox regression. Variables were entered in the model using enter mode. The Mayo right heart score was based on the NYHA class, NT-proBNP and RVLS. The Stanford right heart score was based on the NYHA class, NT-proBNP and RVESRI. The REVEAL score was based on the Registry to Evaluate Early And Long-term PAH Disease Management (REVEAL) groups: low, average, moderate high, high, very high. **p<0.01, *p<0.05. NYHA: New York Heart Association; RVESRI: right ventricular end-systolic remodeling index; RVLS: right ventricular longitudinal strain.

Figure 4. Immunoblot of the protein expression of hepatic growth factor (HGF), its receptor c-Met, Nerve growth factor (NGF) and its receptor TRKA, Stem Cell Growth Factor beta (SCGFb) and SDF1 in the right ventricle of patients with pulmonary arterial

hypertension (PAH) and controls, and quantification of the signal. Each bar represents the mean ± SEM signal intensity of Western Blots lysate from right ventricular samples from 4 PAH undergoing heart-lung transplant and 5 control patients (heart donors), which were compared using Student t-test.

Figure 5. Localization of c-Met (A, red) and its ligand HGF (B, red) in right ventricular biopsies from a patient with idiopathic pulmonary arterial hypertension by immunostaining, double-labeled with either TNNT2 troponin (cardiomyocyte), α-SMA (smooth muscle cell), CD31 (endothelial cells), vimentin VMTN (fibroblast) or CD68 (macrophage) in green, from left to right. No immunoreactivity was seen in cells incubated with the secondary antibody but no primary antibody. Scale bar = 10 μm. DAPI = 4′,6′-diamidino-2-phenylindole.

TABLES

Table 1. Circulating proteomic biomarkers assessed in the study using flow cytometry multiplex arrays.

Class	Biomarkers
Interleukins (IL-)	IL-1α, -1β, -2, -3, -4, -5, -6, LIF, IL-7, -9, -10, -12p70, - 13, -15, -16, -17, -18
Interleukin receptors	IL-1Rα, -2Rα
Chemokines	MCP1=CCL2, MIP1α=CCL3, MIP1β=CCL4, RANTES=CCL5, MCP3=CCL7, CTACK=CCL27, Eotaxin, GROa=CXCL1, IL-8=CXCL8, MIG=CXCL9, IP10=CXCL10, SDF1=CXCL12
Growth factors	MCSF (Macrophage colony-stimulating factor)=CSF1 (Colony stimulating factor 1), NGF (Nerve growth factor), SCF (Stem cell factor), SCGFβ (Stem cell growth factor beta), TNFα (Tumor necrosis factor alpha), TNFβ (Tumor necrosis factor beta 1), HGF (Hepatic growth factor), PDGFbb (Platelet-derived growth factor bb), FGF2=FGFβ (Basic fibroblast growth factor), GCSF (Granulocyte colony-stimulating factor), GMCSF (Granulocyte-macrophages colony-stimulating factor), VEGF-A (Vascular endothelial growth factor-A)
Other cytokines	MIF (Macrophage migration inhibitory factor), TRAIL

(TNF-related apoptosis-inducing ligand), IFNA2 (Interferon alpha-2), IFNγ (Interferon gamma)

Table 2. Comparative baseline characteristics of the discovery and validation cohorts.

Variables	**Discovery cohort n=121**	**Validation cohort n=76**	**p value**
Age (years)	50 [39 – 59]	52 [43 – 61]	0.20
Female sex	90 (74.4)	66 (86.8)	0.06
Race, ethnicity			0.06
White, non-Hispanic	72 (59.5)	41 (53.9)	
Hispanic	20 (16.5)	15 (19.7)	
Asian	22 (18.2)	7 (9.2)	
Black, non-Hispanic	4 (3.3)	6 (7.9)	
Other	3 (2.5)	7 (9.2)	
Body mass index (kg/m^2)	26.9 [22.5 – 31.9]	27.4 [24.7 – 33.5]	0.12
PAH etiology			0.40
Connective tissue disease	40 (33.1)	31 (40.8)	
Idiopathic	34 (28.1)	14 (18.4)	
Drugs and toxins	21 (17.4)	18 (23.7)	
Congenital heart disease	13 (10.7)	7 (9.2)	
Portal pulmonary hypertension	11 (9.1)	5 (6.6)	
Heritable PAH	2 (1.7)	1 (1.3)	
NYHA functional class			0.26
Class I	8 (6.6)	5 (6.6)	
Class II	48 (39.7)	20 (26.3)	
Class III	50 (41.3)	41 (53.9)	

Class IV	15 (12.4)	10 (13.2)	
Six minute walk distance (m)	427 [342 – 537]	392 [299 – 476]	**0.03**
NT-proBNP (pg/mL)	235 [67 – 977]	536 [150 – 1441]	**0.04**
Diffusing capacity of lung for carbon monoxide, DLCO (% predicted)	73 [60 – 86]	69 [53 – 92]	0.91
MDRD estimated glomerular filtration rate (mL/min/1.73m^2)	68 [53 – 90]	66 [54 – 79]	0.21
Hemodynamics			
Right atrial pressure (mmHg)	7 [5 – 11]	7 [5 – 12]	0.49
Mean pulmonary arterial pressure (mmHg)	50 [40 – 59]	49 [40 – 58]	0.78
Pulmonary arterial wedge pressure (mmHg)	10 [8 – 13]	10 [7 – 14]	0.72
Pulmonary vascular resistance (WU)	9.9 [6.1 – 14.2]	10.3 [6.8 – 15.7]	0.56
Cardiac Index (L/min/m^2)	2.2 [1.8 – 2.5]	2.0 [1.6 – 2.3]	**0.03**
Echocardiographic metrics			
RVESAI (cm^2/m^2)	12.7 [10.5 – 16.4]	12.9 [10.2 – 16.2]	0.81
RVESRI	1.4 [1.3 – 1.6]	1.5 [1.3 – 1.6]	0.43
RVLS (absolute value, %)	16.9 [13.9 – 20.0]	16.6 [13.2 – 21.1]	0.93
RVFAC (%)	27.1 [22.7 – 30.7]	26.6 [23.1 – 32.8]	0.91
TAPSE (cm)	1.8 [1.4 – 2.1]	1.7 [1.3 – 2.0]	0.20

PAH Therapy			
Therapy extent			**<0.01**
Treatment naive	35 (28.9)	38 (50.0)	
Monotherapy	34 (28.1)	24 (31.6)	
Dual therapy	36 (29.8)	12 (15.8)	
Triple therapy	16 (13.2)	2 (2.6)	
Phosphodiesterase-5 inhibitors	62 (51.2)	28 (36.8)	**0.04**
Endothelin receptor antagonists	39 (32.2)	12 (15.8)	**0.01**
Prostanoid therapy	53 (43.8)	14 (18.4)	**<0.01**
REVEAL Risk Score			0.48
Low	74 (61.2)	46 (60.5)	
Average/Moderate High Risk	17 (14.0)	15 (19.7)	
High/Very High	30 (24.8)	15 (19.7)	
Mayo Right Heart Score			0.85
Low score (0-5)	50 (41.3)	33 (43.3)	
Intermediate score (6-8)	40 (33.1)	28 (36.8)	
High score (>9)	24 (19.8)	15 (19.7)	
Stanford Right Heart Score			0.72
Low score (0-2)	49 (40.5)	30 (39.5)	
Intermediate score (3)	46 (38.0)	26 (34.2)	
High score (>4)	26 (21.5)	20 (26.3)	

Values are expressed as mean ±SD or number (percentage), or median and interquartile range (IQ). Significant p values (<0.05) are presented as bold. RVSP was estimated from the TR signal

in 194 (85% patients). NT-proBNP: N-terminal pro-b type natriuretic peptide; NYHA: New York Heart Association; PAH: pulmonary arterial hypertension; RV: right ventricular; RVESAI: RV end-systolic area indexed on body surface area; RVESRI: RV end-systolic remodeling index: RVFAC: fractional area change; RVLS: RV free-wall longitudinal strain; RVSP: right ventricular systolic pressure; TAPSE: tricuspid annular plane systolic excursion.

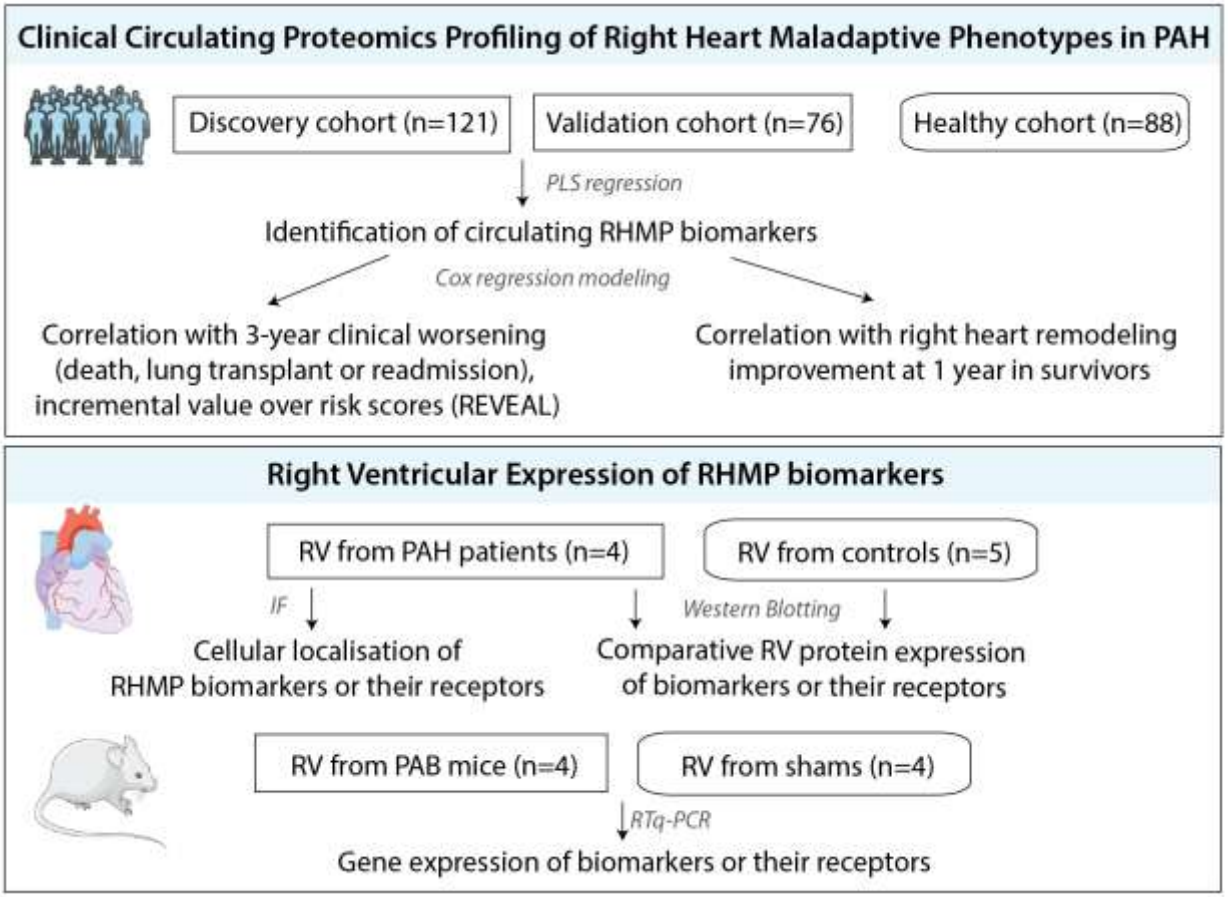
Clinical Circulating Proteomics Profiling of Right Heart Maladaptive Phenotypes in PAH
Discovery cohort (n=121)
Validation cohort (n=76)
Healthy cohort (n=88)
PLS regression
Identification of circulating RHMP biomarkers
Cox regression modeling
Correlation with 3-year clinical worsening (death, lung transplant or readmission), incremental value over risk scores (REVEAL)
Correlation with right heart remodeling improvement at 1 year in survivors
Right Ventricular Expression of RHMP biomarkers
RV from PAH patients (n=4)
RV from controls (n=5)
IF
Western Blotting
Cellular localisation of RHMP biomarkers or their receptors
Comparative RV protein expression of biomarkers or their receptors
RV from PAB mice (n=4)
RV from shams (n=4)
RTq-PCR
Gene expression of biomarkers or their receptors

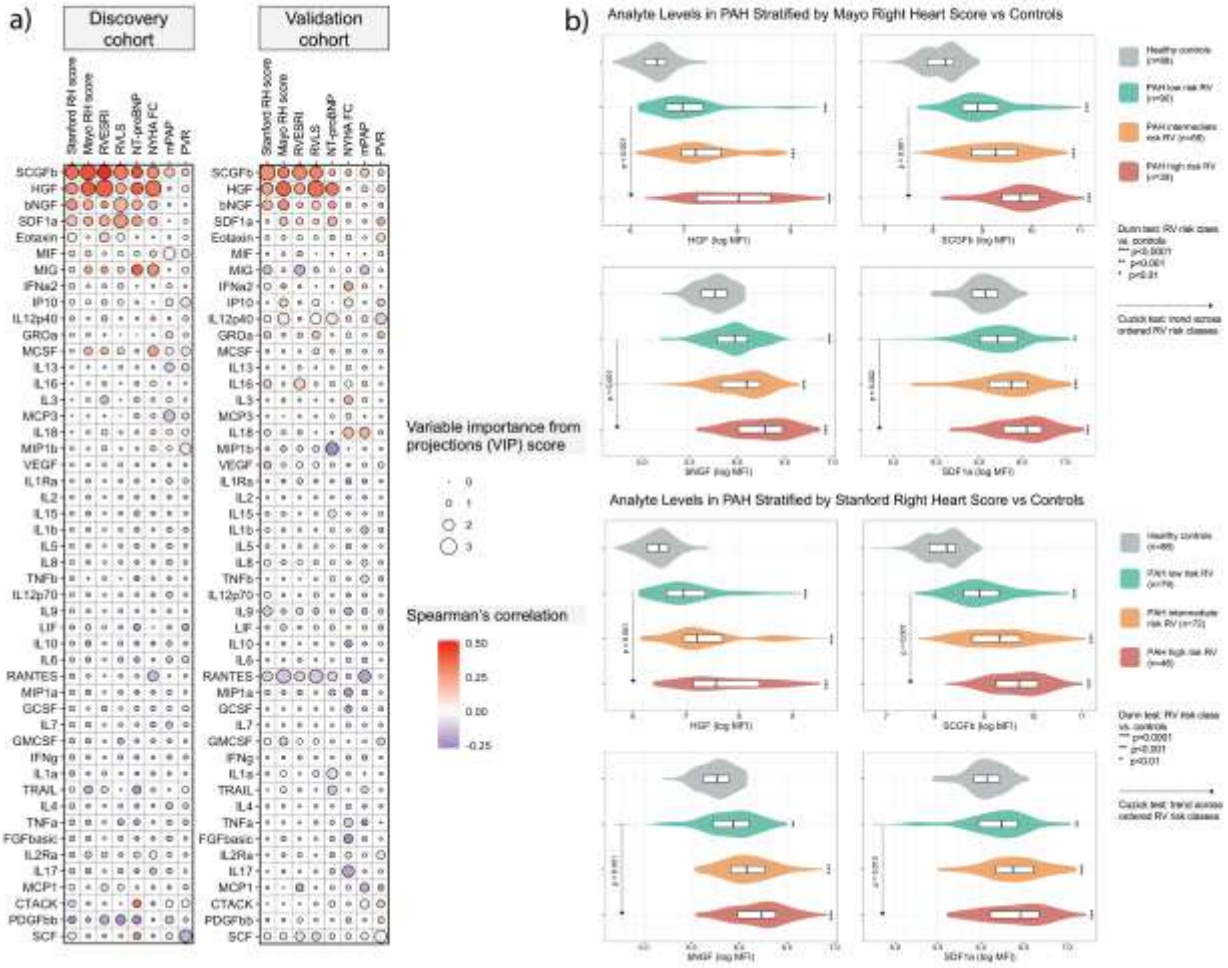
a)
Discovery cohort
Validation cohort
Stanford RH score
Mayo RH score
RVESRI
RVLS
NT-proBNP
NYHA FC
mPAP
PVR
SCGFb
HGF
bNGF
SDF1a
Eotaxin
MIF
MIG
IFNa2
IP10
IL12p40
GROa
MCSF
IL13
IL16
IL3
MCP3
IL18
MIP1b
VEGF
IL1Ra
IL2
IL15
IL1b
IL5
IL8
TNFb
IL12p70
IL9
LIF
IL10
IL6
RANTES
MIP1a
GCSF
IL7
GMCSF
IFNg
IL1a
TRAIL
IL4
TNFa
FGFbasic
IL2Ra
IL17
MCP1
CTACK
PDGFbb
SCF
Variable importance from projections (VIP) score
0
1
2
3
Spearman's correlation
0.50
0.25
0.00
-0.25
b)
Analyte Levels in PAH Stratified by Mayo Right Heart Score vs Controls
HGF (log MFI)
SCGFb (log MFI)
bNGF (log MFI)
SDF1a (log MFI)
Healthy controls (n=68)
PAH low risk RV (n=90)
PAH intermediate risk RV (n=68)
PAH high risk RV (n=38)
Dunn test: RV risk class vs. controls
*** p<0.0001
** p<0.001
* p<0.01
Cuzick test: trend across ordered RV risk classes
Analyte Levels in PAH Stratified by Stanford Right Heart Score vs Controls
HGF (log MFI)
SCGFb (log MFI)
bNGF (log MFI)
SDF1a (log MFI)
Healthy controls (n=68)
PAH low risk RV (n=79)
PAH intermediate risk RV (n=72)
PAH high risk RV (n=46)
Dunn test: RV risk class vs. controls
*** p<0.0001
** p<0.001
* p<0.01
Cuzick test: trend across ordered RV risk classes

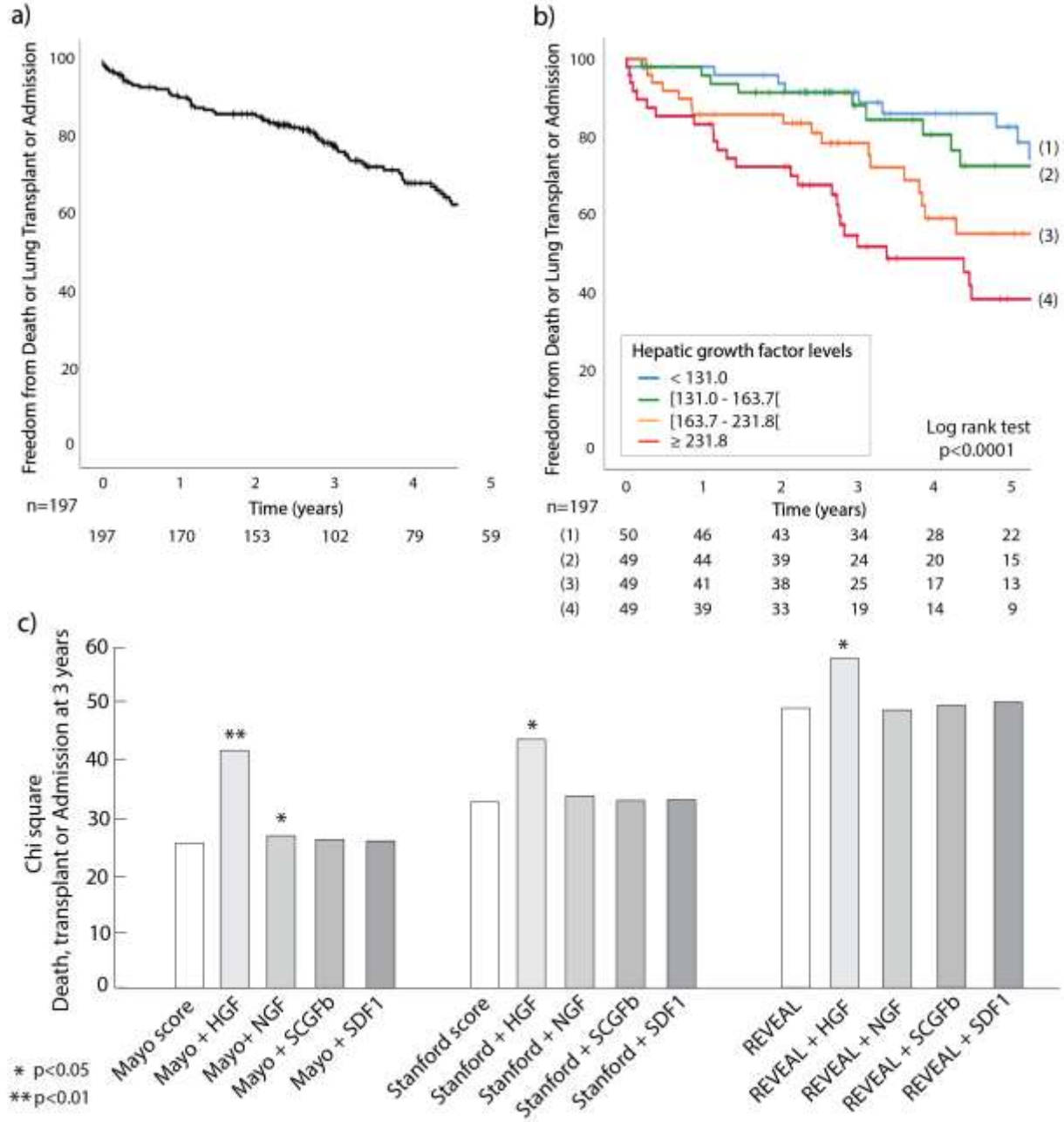
a)
Freedom from Death or Lung Transplant or Admission
100
80
60
40
20
0
0 1 2 3 4 5
Time (years)
n=197
197 170 153 102 79 59
b)
Freedom from Death or Lung Transplant or Admission
Hepatic growth factor levels
< 131.0
[131.0 - 163.7[
[163.7 - 231.8[
≥ 231.8
(1)
(2)
(3)
(4)
Log rank test
p<0.0001
n=197
Time (years)
(1) 50 46 43 34 28 22
(2) 49 44 39 24 20 15
(3) 49 41 38 25 17 13
(4) 49 39 33 19 14 9
c)
Chi square
Death, transplant or Admission at 3 years
60
50
40
30
20
10
0
**
*
*
*
Mayo score
Mayo + HGF
Mayo+ NGF
Mayo + SCGFb
Mayo + SDF1
Stanford score
Stanford + HGF
Stanford + NGF
Stanford + SCGFb
Stanford + SDF1
REVEAL
REVEAL + HGF
REVEAL + NGF
REVEAL + SCGFb
REVEAL + SDF1
* p<0.05
**p<0.01

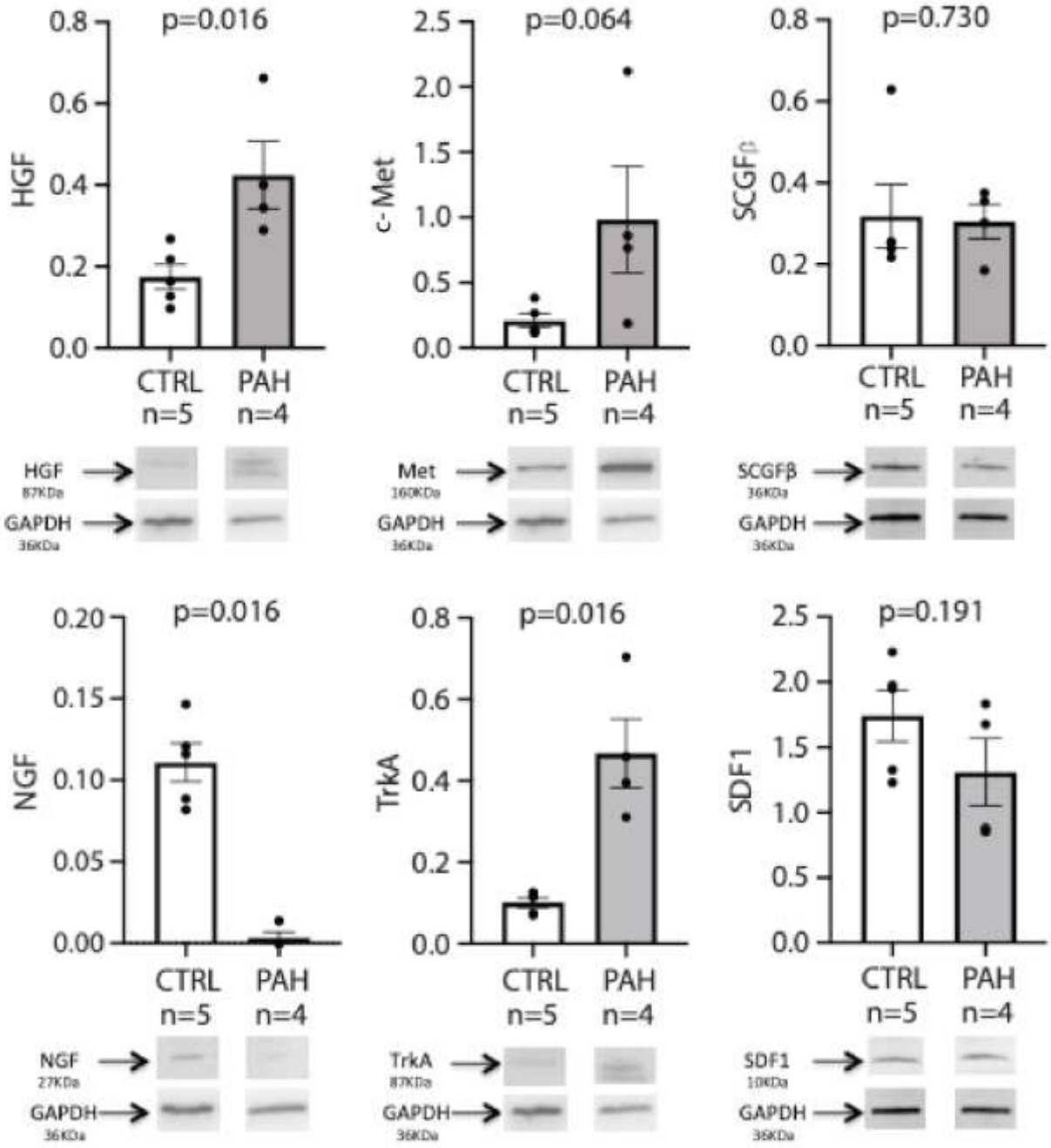
HGF
p=0.016
0.8
0.6
0.4
0.2
0.0
CTRL
n=5
PAH
n=4
HGF
87KDa
GAPDH
36KDa
c-Met
p=0.064
2.5
2.0
1.5
1.0
0.5
0.0
CTRL
n=5
PAH
n=4
Met
160KDa
GAPDH
36KDa
SCGFβ
p=0.730
0.8
0.6
0.4
0.2
0.0
CTRL
n=5
PAH
n=4
SCGFβ
36KDa
GAPDH
36KDa
NGF
p=0.016
0.20
0.15
0.10
0.05
0.00
CTRL
n=5
PAH
n=4
NGF
27KDa
GAPDH
36KDa
TrkA
p=0.016
0.8
0.6
0.4
0.2
0.0
CTRL
n=5
PAH
n=4
TrkA
87KDa
GAPDH
36KDa
SDF1
p=0.191
2.5
2.0
1.5
1.0
0.5
0.0
CTRL
n=5
PAH
n=4
SDF1
10KDa
GAPDH
36KDa

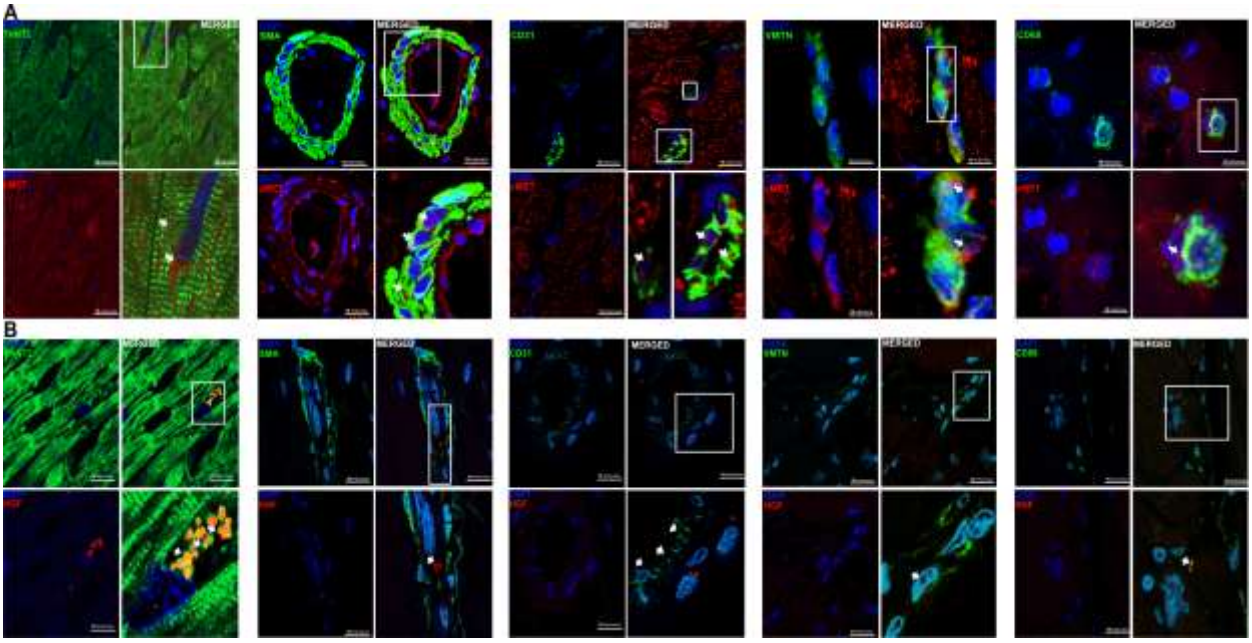
A
TNNT2
MERGED
SMA
MERGED
CD31
MERGED
VIMTN
MERGED
CD68
MERGED
B
SMA
MERGED
CD31
MERGED
VIMTN
MERGED
CD68
MERGED

ONLINE DATA SUPPLEMENT

Targeted Immune and Growth Factor Proteomics of Right Heart Adaptation to Pulmonary Arterial Hypertension

Myriam Amsallem MD PhD[a,b,c*], Andrew J. Sweatt MD[c,d*], Jennifer Arthur Ataam PhD[a,b,], Julien Guihaire MD PhD[e], Florence Lecerf MS[e], Mélanie Lambert PhD[e], Maria Rosa Ghigna MD PhD[f], Md Khadem Ali PhD[c,d], Yuqiang Mao MD PhD [c,d], Elie Fadel MD PhD[e], Marlene Rabinovitch MD[c,g], Vinicio de Jesus Perez MD PhD[c,d], Edda Spiekerkoetter MD[c,d], Olaf Mercier MD PhD[e], Francois Haddad MD[a,b,c*], Roham T. Zamanian MD[c,d*]

Supplementary Methods

1) Plasma sample collection, processing and biorepository storage

Pulmonary arterial hypertension. PAH samples were obtained from the Stanford Pulmonary Hypertension Biobank (Stanford University, CA, USA), which is a comprehensive tissue bank that includes plasma, serum, peripheral blood mononuclear cells, exhaled breath condensate, and urine from patients with all forms of pulmonary hypertension (Stanford University IRB #14083). Initiated in 2007, the Stanford Pulmonary Hypertension Biobank has captured samples from over 600 well-characterized subjects who were recruited at the time of evaluation in Stanford Pulmonary Hypertension clinic. After informed consent was obtained, study plasma samples were collected from patients during right heart catheterization in the fasting state. Peripheral blood was drawn from the antecubital fossa into EDTA vacutainers under standard sterile precautions. Collection tubes were immediately placed upright into a rack at room temperature. Within 30 minutes, the sample was inverted several times to mix components, and subsequently centrifuged at 1300 rpm for 10 minutes. The plasma layer was then carefully removed by pipette without disturbing the buffy coat, and transferred to Eppendorf tubes in 200µL aliquots.

Aliquoted samples were secured and stored upright at -80°C in the Stanford Pulmonary Hypertension Biobank.

Healthy controls. Control plasma samples (n=88) were acquired from the Stanford Cardiovascular Institute Biomarker and Phenotype Core Laboratory biorepository (Stanford University #40869). Samples were collected from healthy volunteers between 2009 and 2013, as part of the Stanford Healthy Aging Study (Stanford University IRB #20942). Peripheral venous blood was drawn in the fasting state from the antecubital fossa, and subsequently processed and stored utilizing the same protocol and conditions that were applied for PAH samples (see above). To establish health in these individuals, initial screening involved a comprehensive questionnaire and clinical assessment with blood pressure and anthropometric measurements. Subjects were excluded for any unexplained chronic cardiopulmonary symptoms (dyspnea, cough, angina, palpitations, orthopnea, lightheadedness), symptomatic atherosclerotic disease, symptomatic heart failure, history of atrial fibrillation, hypertension, chronic pulmonary disease, diabetes mellitus requiring therapy, current smoking, hyperlipidemia requiring therapy, body mass index above 35kg/m2, history of atopy, chronic systemic inflammatory disease, recent infectious disease, prior or current malignancy, and Alzheimer's disease. Subjects had basic laboratory studies to rule out dyslipidemia, elevated NT-proBNP (above or equal to 300 pg/mL), abnormal liver function tests, and renal dysfunction (stage 3 or greater). The participants were then screened with vascular ultrasound for abdominal aortic aneurysm (5cm or greater) and asymptomatic carotid or femoral atherosclerosis (20% or greater diameter stenosis). Transthoracic echocardiography was also employed to screen and exclude those with subclinical left ventricular dysfunction (ejection fraction <50%), subclinical valvular heart disease

(categorized as mild or greater), any right ventricular enlargement or dysfunction, or estimated right ventricular systolic pressure 30mmHg or greater).

2) Multiplex immunoassay blood proteomic profiling

Immunoassay sample and plate preparation. The Luminex 200™ plate reader instrument was calibrated according to manufacturer instructions. This process employed Bio-Plex calibration beads to standardize fluorescent signal detection. To prepare experimental samples, frozen biobanked plasma aliquots were passively thawed to room temperature and diluted four-fold in assay buffer (1 volume plasma to 3 volumes buffer). These plasma samples were assayed within 30 minutes of reaching room temperature, as described below. To prepare a magnetic capture bead mixture, bead stock solution (20x) was vortexed at medium speed for 30 seconds and then diluted 20-fold in assay buffer. The preparation of standards involved first adding 500⌈L of standard diluent to each stock vial of lyophilized standard, which contained known concentrations of analytes measured by our assay. The reconstituted standard was vortexed and incubated on ice for 30 minutes. Thereafter, we performed four-fold serial dilution to prepare a series of eight total standards.

Immunoassay execution. After preparation of the samples, capture bead mixture, and standards, the immunoassay was carried out on a 96-well plate. First, we added 75 ⌈L of standard to eight wells (one standard dilution per well), 75 ⌈L of assay buffer to one well ('blank' well without sample later used to measure background fluorescence from non-specific binding), and a 75 ⌈L pre-diluted experimental sample to the remaining wells. Next, we added 25 ⌈L of capture bead mixture to all plate wells. The plate was sealed, placed on a shaker for two hours (800 rpm), and incubated at 4°C overnight. After passive re-warming the next day, solution was removed and

the plate was washed by magnetic separation with the Bio-Plex Pro™ wash station (200 ⌈L buffer, 3 cycles). Biotinylated detection antibody stock solution (10x) was diluted 10-fold in assay buffer and added to each well (25 ⌈L), followed by two-hour incubation on a shaker (800 rpm), solution removal, and three magnetic separation washes. Next, streptavidin-phycoerythrin stock solution (100x) was diluted 100-fold, incubated in each well (50 ⌈L) for 40 minutes on a shaker (500 rpm), removed, and the plate was washed again. Finally, after addition of reading buffer (100 ⌈L) and ten-minute incubation on a shaker (800 rpm), the plate was read by a Luminex 200™ dual-laser detection instrument. Data acquisition was set to a 50-bead count minimum per analyte per well. Data was processed and presented with Bio-plex Manager™ software.

3) Echocardiographic RV phenotyping of PAH patients

Digitized echocardiographic studies were acquired by the Stanford Biomarker and Phenotypic Laboratory, using Philips IE 33 ultrasound systems (Philips, Amsterdam, The Netherlands). All measures were averaged over three cycles, performed according to the latest American Society of Echocardiography guidelines (22,23) and assessed off-line by two blinded certified readers, as recently described (3). Right heart dimensions and functional metrics were measured on RV-focused apical 4-chamber views (24). RV end-systolic area was indexed on ideal body weight-adjusted body surface area (RVESAI). RV end-systolic remodeling index (RVESRI) was defined by the lateral wall to septal height ratio (3). RV function was assessed using free-wall Lagrangian longitudinal strain (RVLS, measured from mid-endocardial end-diastolic and end-systolic manually traced lengths), RV fractional area change (RVFAC) and tricuspid annular plane systolic excursion (TAPSE).

Follow-up echocardiograms available in survivors at 1 year were available in 174 patients (93% of 1-year survivors). These echocardiograms were interpreted using the same methodology. Right heart remodeling with therapy was defined using changes in RVESRI from baseline echocardiograms, as previously published in Amsallem et al. Circulation Cardiovascular Imaging, 2017 (1). Improvement in RVESRI was defined by a relative delta <10% between the baseline and follow-up echo, worsening if >10% and stable otherwise. Binary logistic regression analyses were used to assess whether baseline levels of HGF, NGF, SCGFb or SDF1 were associated with the end point of improvement in RVESRI at 1 year. To explore the predictive value of these biomarkers stratifying on the therapy initiated or changes in PH-specific therapy between baseline and follow-up, we performed binary logistic regression analyses in the three following subgroups: [1] patients in whom parenteral prostanoids were initiated between baseline and follow-up, [2] patients in whom there was no change in PH-specific therapies (including ERA, PDE5I, or oral prostanoids) and [3] others.

4) Histological analysis of human RV tissue

Right ventricular myocardial samples from the 4 patients with PAH were embedded in paraffin for histological study. They were cut in 4 μm-thick sections and stained with 0.1% Picro-Sirius Red for histological evaluation of fibrosis on a single slice. Histological image processing was performed using Nikon NIS-Elements (Tokio, Japan). Quantification of fibrosis from histological images was performed using semi-automated segmentation through a multi-channel thresholding method based on the color and illumination contents (using ImageJ software v.1.4, NIH, Bethesda, MD). The histology images were first manually determined by outlines, which defined each tissue component separately. Artifacts and objects of non-interest (background,

perivascular, endocardial fibrosis, and epicardial fibrosis) were manually delineated from the selected area. The quantitative results were expressed as the surface area for myocardium and fibrosis.

5) Western blots: protein quantification in human RV tissue

Western blots were performed on frozen samples from right ventricles of 4 patients with PAH and 5 controls to compare protein levels of the 4 biomarkers (HGF, NGF, SCGFbeta or SDF1) or their known receptors (c-Met, TrkA). RV biopsies were lysed and sonicated in RIPA buffer supplemented with protease/phosphatase inhibitor cocktail. Following agitation for 1h at 4°C, the lysate was obtained after centrifugation at 4000 g for 10 minutes at 4°C. Protein concentration in lysates was determined by BCA protein assay kit (Thermo Scientific, Rockford, IL); 40 µg of total proteins were separated on 4–20% sodium dodecyl sulfate-polyacrylamide gel electrophoresis gels (Criterion, Biorad). Proteins were transferred to polyvinylidene difluoride or nitrocellulose membranes (Hybond, Amersham) and blocked for 1 hour at room temperature with 5% nonfat dry milk in Tris-buffered saline plus 0.1% Tween 20. Incubation with specific primary antibodies presented in the table below was performed in a blocking buffer overnight at 4°C. Horseradish peroxidase–conjugated anti-mouse IgG (7076, cell signaling) or anti-rabbit IgG (7074, cell signaling) was used as secondary antibody and incubate 1h, in blocking buffer, at room temperature. Immunoreactive bands were detected using ECL chemiluminescent substrate (RPN2236, amersham). Membrane stripping was done by incubating the membrane in Restore Western blot stripping buffer (Thermo Scientific) according to the manufacturer's instructions. Relative expression was expressed by normalizing the protein of interest to the Glyceraldehyde 3-phosphate dehydrogenase (GAPDH).

Anticorps	Species	Reference	Dilution
anti-HGF polyclonal antibody	Rabbit	ab83760, Abcam	1/1000
Recombinant anti-c-Met antibody	Rabbit	ab51067, Abcam	1/1000
anti-NGF antibody	Rabbit	ab6199, Abcam	1/500
recombinant anti-TrkA antibody	Rabbit	ab76291, Abcam	1/500
anti-SDF1 polyclonal antibody	Rabbit	ab9797, Abcam	1/1000
anti-SCGFb antibody	Mouse	ab90238, Abcam	1/250

Incubation with specific primary antibodies (all Abcam, Cambridge, UK): anti-HGF polyclonal antibody (ab83760), recombinant anti-c-Met antibody (ab51067), anti-NGF antibody (ab6199), recombinant anti-TrkA antibody (ab76291), anti-SDF1 polyclonal antibody (ab9797) and anti-SCGFβ antibody (ab90238) were performed in blocking buffer overnight at +4°C. Horseradish peroxidase–conjugated anti-IgG was used as a secondary antibody. Immunoreactive bands were detected by ECL chemiluminescent substrate (Perkin Elmer). If needed, membrane stripping was done by incubating the membrane in the Restore Western blot stripping buffer (Thermo Scientific) according to the manufacturer's instructions. Relative expression was expressed by normalizing the protein of interest to the Glyceraldehyde 3-phosphate dehydrogenase (GAPDH).

6) Immunofluorescence: protein localization in human RV tissue

Paraffin embedded RV slices (5 µm) were deparaffinized in toluene and rehydrated in baths of decreasing concentration of ethanol, prior to water baths. Then unmasking was performed using

two unmasking baths with different pH (pH6 or pH9), depending on the primary antibody used. Sections were saturated with BSA (0.1%) and goat serum (10%), diluted in PBS, for 1 h at room temperature. They were then incubated overnight at 4°C with the primary antibodies presented in the table below, washed with PBS, before incubation with the secondary antibody presented in table 2, 1h at room temperature. Slides were counterstained with 4',6'-diamidino-2-phenylindole (DAPI). Each slide was visualized with a confocal microscope Zeiss (LSM 800) and processed with ZEN software (Carl Zeiss Microscopy, NY, USA).

Anticorps	**Species**	**Reference**	**Dilution**	**pH of unmasking bath**
Anti-HGF polyclonal antibody	Rabbit	ab83760, Abcam	1/100	9
Recombinant anti-c-Met antibody	Rabbit	ab51067, Abcam	1/100	9
Anti-NGF antibody	Rabbit	ab6199, Abcam	1/100	6
Recombinant anti-TrkA antibody	Rabbit	ab76291, Abcam	1/100	9
Anti-SDF1 polyclonal antibody	Rabbit	ab9797, Abcam	1/100	6

Anti-SCGFb antibody	Mouse	ab90238, Abcam	1/100	9
Anti-CD31 antibody	Mouse	M0823, Clone JC70A, Dako	1/50	6 & 9
Anti-CD31 antibody	Rabbit	ab28364, Abcam	1/50	9
Anti-CD68 antibody	Mouse	ab955, Abcam	1/100	6 & 9
Anti-CD68 antibody	Rabbit	ab125212, Abcam	1/100	9
Anti-Vimentin antibody	Mouse	ab8978, Abcam	1/100	6 & 9
Anti-TNNT2	Mouse	A25969, life technologies	1/50	6 & 9
Anti-α-SMA -FITC	Mouse	clone 1A4, Sigma-Aldrich	1/400	6 & 9
Anti-rabbit (594)	Goat	A11037, invitrogen	1/400	6 & 9
Anti-mouse (594)	Goat	A11032, invitrogen	1/400	6 & 9

Anti-rabbit (488)	Goat	A11034, invitrogen	1/400	6 & 9
Anti-mouse (488)	Goat	A11029, invitrogen	1/400	6 & 9

7) Pulmonary arterial banding (PAB) mouse experimental model

All animal experiments were performed in accordance with National Research Council guidelines (*Guide for Care and Use of Laboratory Animals*) and approved by local authorities (APLAC, Stanford University, Protocol #27626). Experiments were conducted in a blinded fashion whenever possible (i.e. exercise testing, haemodynamics measurements, or histological analysis). The PAB model was established to induce chronic RV pressure overload in 10-14-week-old male C57BL/6 mice, as previously published (2). All mice were anesthetized with 0.05–0.1 mg/mg Buprenorphine subcutaneously along with continuous Isoflurane (2–3%). A left thoracotomy was performed at the fourth intercostal space, and the main pulmonary artery was exposed with and banded around a 24G needle with 6-0 silk sutures. Maintenance anesthesia was performed using 1% to 2% isoflurane. The sham surgery control group consisted of age-matched littermates who underwent the same procedure, including isolation of the pulmonary artery trunk without placing a suture. One week after surgery, a peak pressure gradient was measured across the PA band with echocardiography (GE Vivid 7) and only mice with peak pressure gradient >15 mmHg were included into the study protocol. After 5 weeks of surgery, pulmonary artery pressure, heart rate, pulmonary valve velocity time integral by echocardiography were measured to document a reduced cardiac output (2), and RV tissues were collected and snap frozen for further use.

8) Gene expression analysis of PAB model RV samples

Total RNA was isolated from homogenized RV of the PAB model using the RNAeasy Plus Kit (Qiagen, Hilden, Germany) and then reverse transcribed into cDNA using SuperScript III (Invitrogen, Carlsbad, CA, USA) according to the manufacturer's instructions. The level of mRNA transcripts for *Hgf*, *c-Met*, *Ngf*, *Scgfβ* were measured in triplicate using a reaction mixture containing TaqMan gene expression master mix and primer/probe sets (Applied Biosystems, Foster City, CA, USA) and normalized to GAPDH (2).

10) Statistical analysis: Partial least squares regression

Partial least squares (PLS) regression overview. PLS regression was chosen given that it can handle a large number of predictor variables and multiple correlated predictors. Several proteomic blood biomarkers were measured (predictors in this study) including mainly cytokines and chemokines, which inherently often exhibit multicollinearity. Briefly, PLS regression involves the extraction of several linear combinations of the predictor variables, called latent factors, which maximize covariance between predictors and the response variable. In other words, the PLS approach finds latent factors which account for as much variation in the predictors as possible while still modeling the response variable. Proteomic data preprocessing involved background fluorescence subtraction, plate/batch adjustment (empirical Bayes methodology) [11], robust quantile normalization, and duplicate averaging, and adjustment for age, sex, and body mass index.

PLS regression implementation. PLS multivariate regression was carried out using the 'pls' R software package (3). PLS models were fit using the SIMPLS algorithm. The SIMPLS method, compared to other PLS algorithms, truly attempts to maximize the covariance criterion when

determining latent factors, and obeys orthogonality and normalization restrictions. SIMPLS analysis avoids the construction of deflated data matrices and is easily interpretable. PLS models were fit to associate measured proteomic predictors with various response variables: Mayo right heart score, Stanford right heart score, individual components of these right heart scores (RVLS, NYHA functional class, NT-proBNP, and RVESRI), and pulmonary hemodynamic measures (mPAP and PVR). Each PLS regression model consisted of the full matrix of proteomic predictors and a right heart score, single RV metric, or clinical response variable. First, models were fit with the full number of components and a leave-one-out cross validation procedure. To select the optimal number of components for inclusion in each model, we evaluated the root mean squared error of prediction (RMSEP) as a function of number of components, and the one-sigma heuristic was applied (4). Then, each model was fit with the fewest number of components that minimized RMSEP. To identify the RHMP proteomic markers, we focused on the models in which the Mayo Clinic right heart score and Stanford right heart score were the response variable. The most significant predictors were identified from (i) variable importance for projection (VIP) scores and regression beta coefficients. VIP scores quantified the importance of each protein marker in the construction of latent factors. Significance testing was performed for the regression coefficients, by using jackknife resampling to obtain coefficient variance estimates and then applying t-tests.

Online Figure Legends

Figure E1. Volcano plots of the partial least square regression analyses of the circulating proteomic biomarkers associated with right heart scores and metrics in both cohorts. The y-axis represents the VIP scores and the x-axis the Spearman correlation coefficient. Red: higher cytokine levels correlate with less favorable risk score or right heart metric (as continuous variables). Green: higher cytokine levels correlate with a more favorable risk score or right heart metric. MPAP: mean pulmonary arterial hypertension; NYHA: New York Heart Association; PVR: pulmonary vascular resistance; RVLS: right ventricular free-wall longitudinal strain is presented in absolute value (lowest values indicate worst right ventricular dysfunction); RVESRI: right ventricular end-systolic remodeling index. For cytokines abbreviations, please see **Table E1**.


Mayo Right Heart Score
Discovery cohort
Validation cohort
Stanford Right Heart Score
Discovery cohort
Validation cohort
RVLS
Discovery cohort
Validation cohort
RVESRI
Discovery cohort
Validation cohort
NT-proBNP
Discovery cohort
Validation cohort
NYHA
Discovery cohort
Validation cohort
MPAP
Discovery cohort
Validation cohort
PVR
Discovery cohort
Validation cohort

Figure E2. Levels of the 4 markers according to gender (a) or ethnicity and race (b). (a) Comparative analyte levels of the 4 biomarkers associated with right heart maladaptive phenotype according to gender in healthy controls (n=88) and in patients with PAH (n=197), using Kruskal Wallis test with post-hoc pairwise comparisons adjusted for multiple testing (Benjamini Hochberg). Male versus female comparison p-values are shown among controls and PAH subjects. **(b)** Comparative analyte levels of the 4 strongest biomarkers associated with right heart maladaptive phenotype according to ethnicity and race groups in the total cohort of patients with PAH (n=197), using Kruskal Wallis test (across-groups) with post-hoc pairwise comparisons adjusted for multiple testing (Benjamini Hochberg). For each marker, the across-group p-value is shown along with only significant ($p<0.05$) pairwise comparisons. The p-values for all other pairwise comparisons not shown were non-significant.

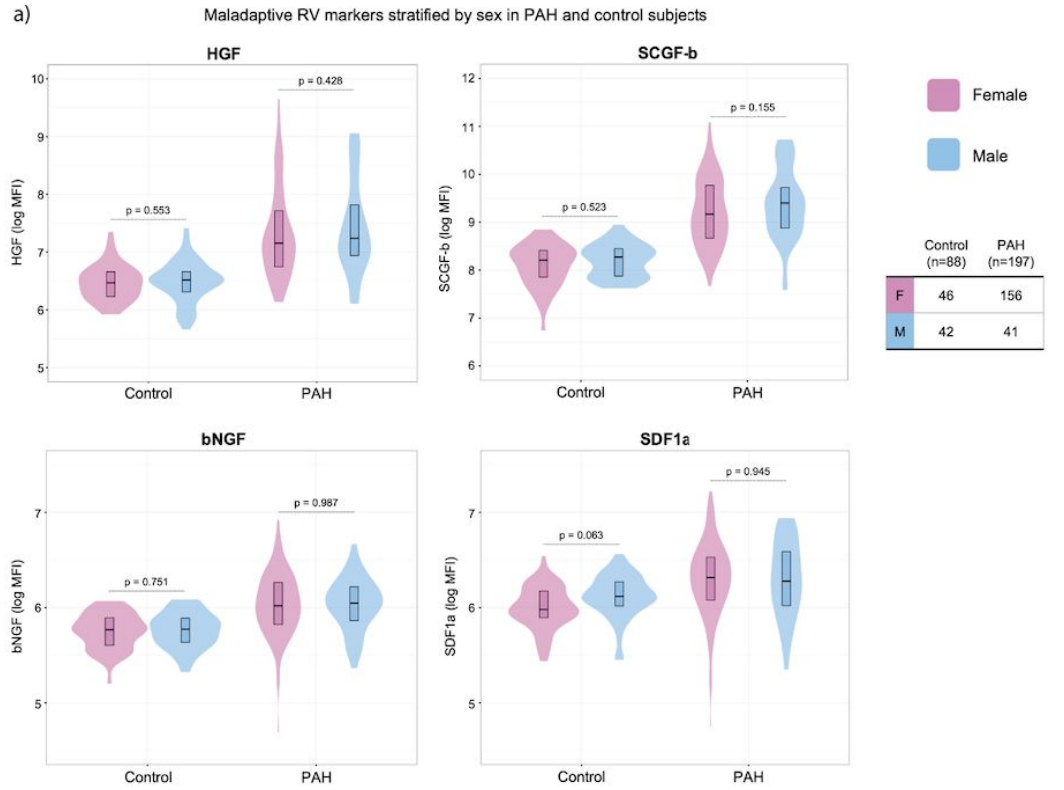
a)
Maladaptive RV markers stratified by sex in PAH and control subjects
HGF
SCGF-b
bNGF
SDF1a
HGF (log MFI)
SCGF-b (log MFI)
bNGF (log MFI)
SDF1a (log MFI)
p = 0.553
p = 0.428
p = 0.523
p = 0.155
p = 0.751
p = 0.987
p = 0.063
p = 0.945
Control
PAH
Female
Male
Control (n=88)
PAH (n=197)
F 46 156
M 42 41

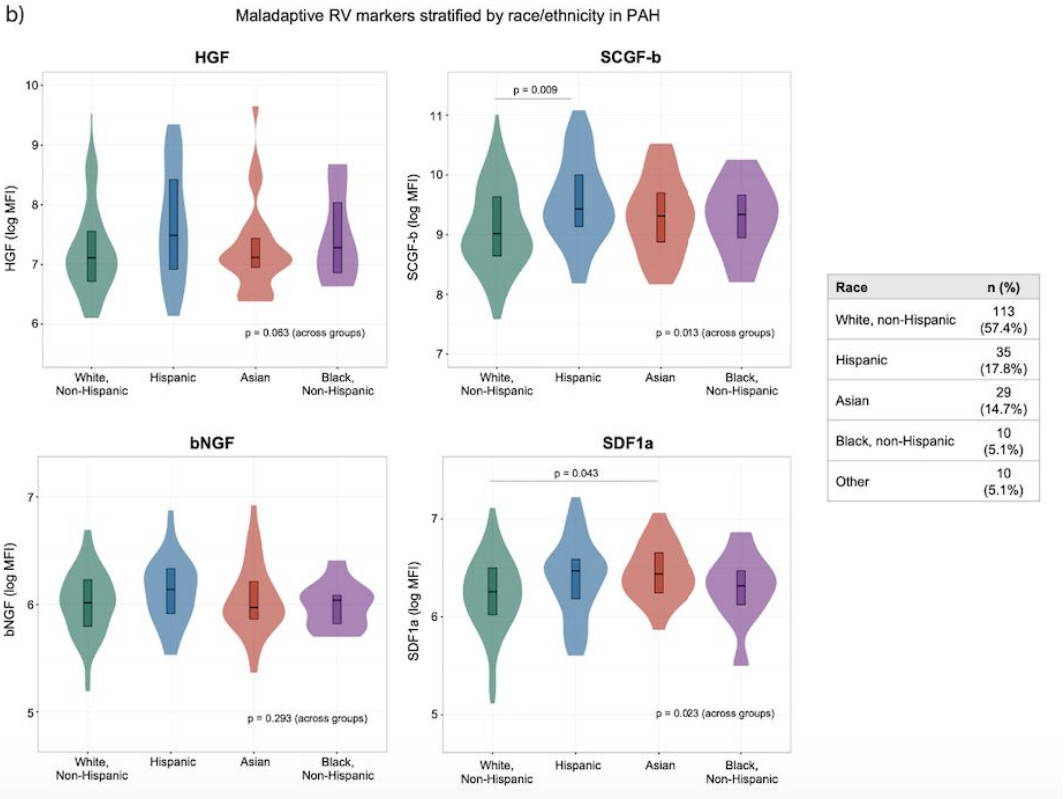
b)
Maladaptive RV markers stratified by race/ethnicity in PAH
HGF
SCGF-b
bNGF
SDF1a
HGF (log MFI)
SCGF-b (log MFI)
bNGF (log MFI)
SDF1a (log MFI)
p = 0.063 (across groups)
p = 0.009
p = 0.013 (across groups)
p = 0.293 (across groups)
p = 0.043
p = 0.023 (across groups)
White, Non-Hispanic
Hispanic
Asian
Black, Non-Hispanic
Race n (%)
White, non-Hispanic 113 (57.4%)
Hispanic 35 (17.8%)
Asian 29 (14.7%)
Black, non-Hispanic 10 (5.1%)
Other 10 (5.1%)

Figure E3. Five-year Kaplan Meier survival curves for the primary combined end point of death, lung transplant or hospitalization for acute right heart failure according to quartiles of stem cell growth factor beta (SCGFβ) levels at baseline.

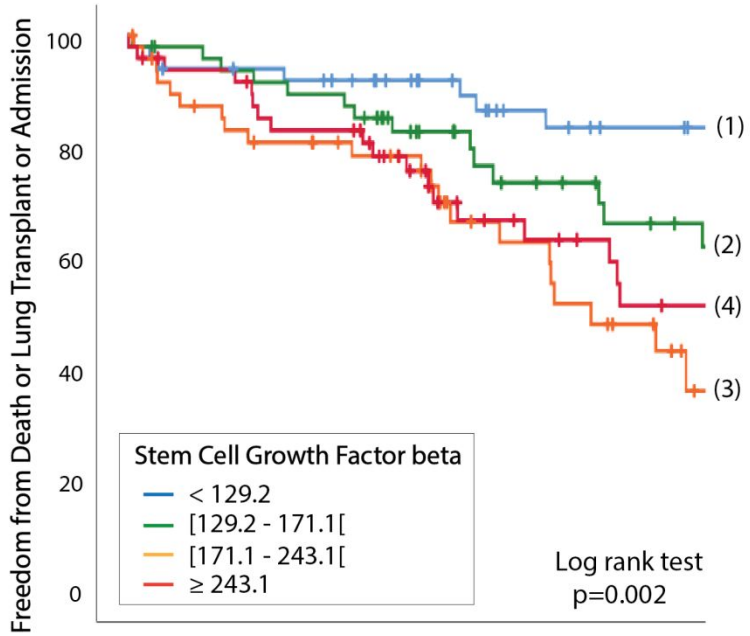

n=197						
(1)	50	45	42	34	27	24
(2)	49	44	41	27	21	16
(3)	49	38	33	19	14	7
(4)	49	43	38	23	17	12

Figure E4. Illustrative right ventricular myocardial biopsies from patients with either idiopathic (left panel) or BMPR2 mutation-related pulmonary arterial hypertension PAH (right panel). Fibrosis levels were measured after Picro-Sirius Red staining, and expressed as the ratio between fibrosis and the total amount of tissue assessed (by determining the total tissue areas occupied by cardiomyocytes and collagen, excluding the lumen). Quantification of fibrosis from histological images was performed using semi-automated segmentation through a multi-channel thresholding method based on the color and illumination contents (using ImageJ software v.1.4, NIH, Bethesda, MD).

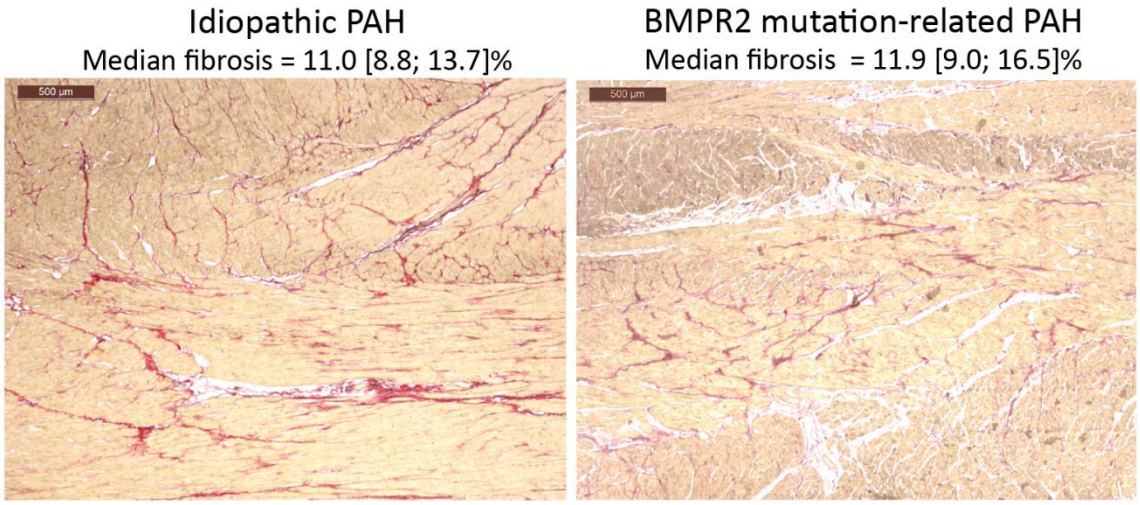

Figure E5. Localization of TrkA (A, red) and its ligand NGF (B, red), SCGFb (C, red) or SDF1 (D, red) in right ventricular biopsies from a patient with idiopathic pulmonary arterial hypertension by immunostaining, double-labeled with either troponin TNNT2 (cardiomyocyte), α-SMA (smooth muscle cell), CD31 (endothelial cells), vimentin VMTN (fibroblast) or CD68 (macrophage) in green, from left to right. No immunoreactivity was seen in cells incubated with the secondary antibody but no primary antibody. Scale bar = 10 μm. DAPI = 4′,6′-diamidino-2-phenylindole.

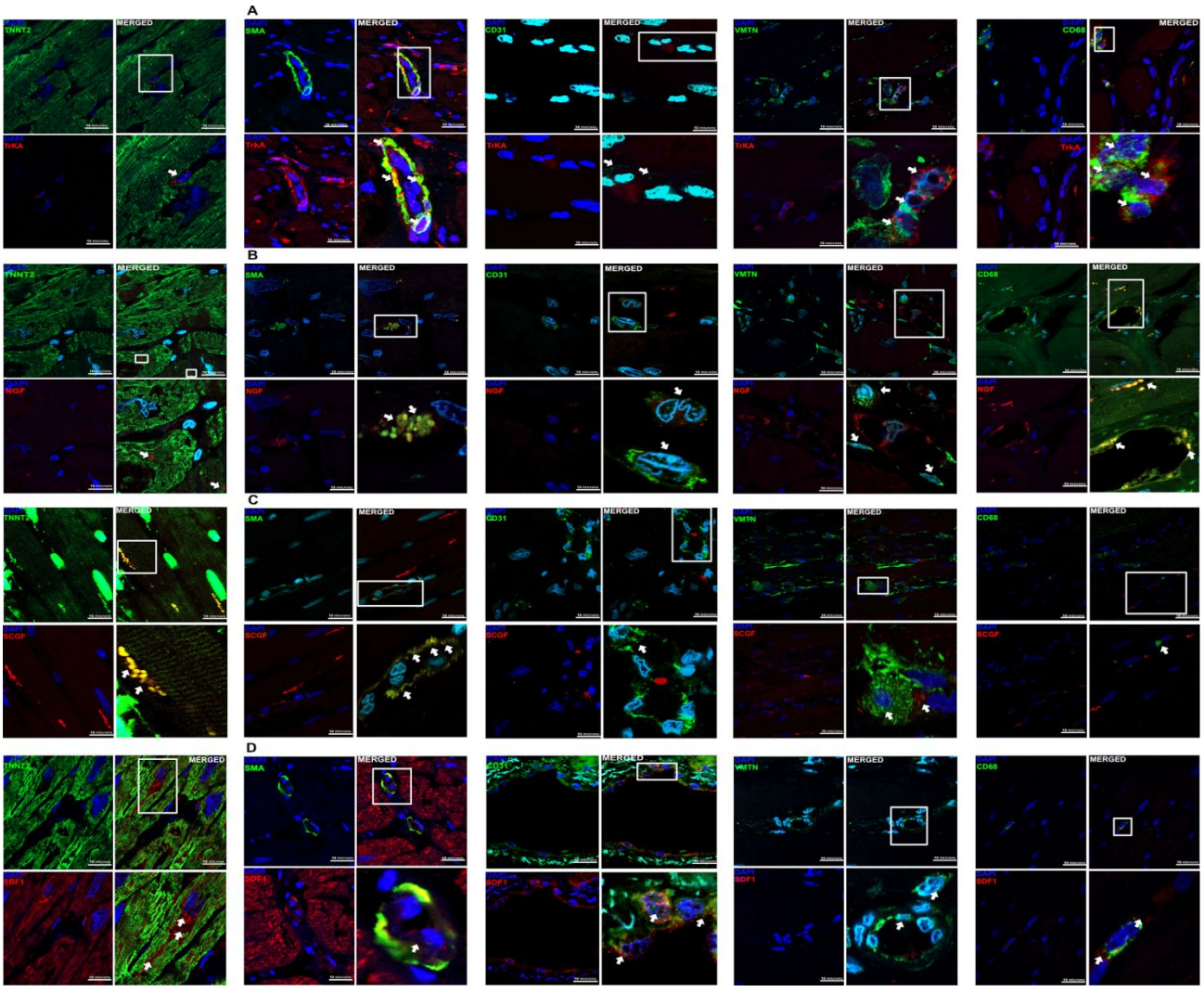

Figure E6. Gene expression of HGF, c-Met, NGF and SCGFb in the RV of pulmonary artery banding mice versus shams. Male C57BL/6 mice (12-14 weeks of age) were anaesthetized and PAB was performed with a non-absorbable silk suture. Five weeks after PAB surgery, right ventricular tissue was collected for gene expression analysis. The RNA expression of *Hgf, c-Met and Ngf* were significantly increased whereas the expression of *Scgfβ* was significantly decreased in right ventricular homogenates from PAB compared to Sham control mice. Data are presented as mean±SEM (n=4/group). Student's 2-tailed, unpaired t-test.

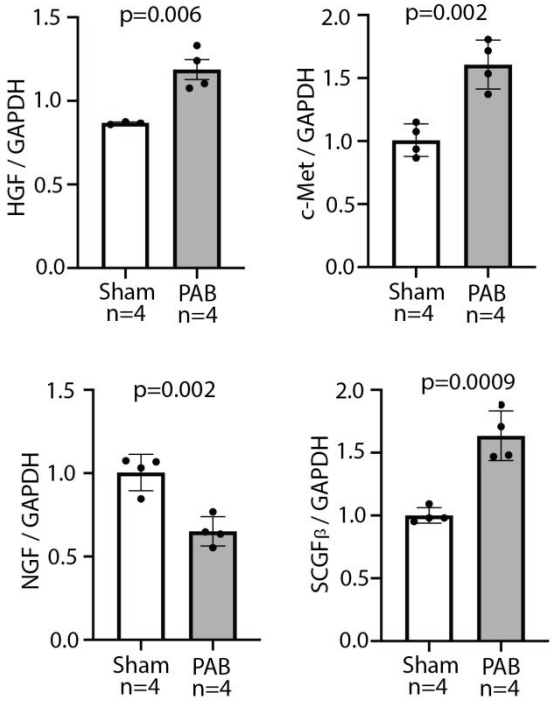

Table E1. Circulating proteomic biomarkers assessed in the study using flow cytometry multiplex arrays (Luminex®). PAH: pulmonary arterial hypertension; PH: pulmonary hypertension.

Abbreviation	Full name	Selected features
Interleukins and receptors		
IL1α	Interleukin-1 alpha	- Pro-inflammatory cytokine - Produced by macrophages, neutrophils and endothelial cells - Induced TNFα release by endothelial cells - Stimulates hepatocytes for CRP secretion - Binds to the interleukin-1 receptor
IL1β	Interleukin-1 beta	- Produced by activated macrophages as a proprotein, which is proteolytically processed to its active form from caspase 1 - Cell proliferation, differentiation and apoptosis
IL2	Interleukin-2	- Promotes the differentiation of immature T-cells into regulatory T-cells, effector T-cells or memory T-cells
IL3	Interleukin-3	- Stimulates proliferation of all cells in the myeloid lineage
IL4	Interleukin-4	- Induces the differentiation of naïve helper T-cells (Th0 cells) to Th2 cells - Decreases the production of Th1 cells and macrophages, promotes M2 repair macrophages > M1
IL5	Interleukin-5	- Produced by type-2 T helper cells and mast cells - Associated with eosinophil and allergy
IL6	Interleukin-6	- Acts as both a pro-inflammatory cytokine (secreted by macrophages and stimulating acute phase protein synthesis and production of neutrophils) and an anti-inflammatory myokine (through inhibitory effects on TNF-alpha and IL-1, and activation of IL-1ra and IL-

		10)
LIF	Leukemia inhibitory factor	- Interleukin-6 class cytokine - Affects cell growth by inhibiting differentiation - Role in cachexia and inflammation
IL7	Interleukin-7	- Hematopoietic growth factor, role in lymphocyte maturation
IL9	Interleukin-9	- Secreted by CD4+ helper cells that acts as a regulator of a variety of hematopoietic cells - Stimulates cell proliferation and prevents apoptosis
IL10	Interleukin-10	- Anti-inflammatory cytokine
IL12p70 IL12p40	Interleukin-12 (p70=active heterodimer) (p40=homodimer)	- Produced by dendritic cells, macrophages, and neutrophils - Promotes the differentiation of naive T cells into Th1 cells, involved in the activation of NK cells and T-cells - Stimulates production of IFNγ and TNFα - Anti-angiogenic activity
IL13	Interleukin-13	- Involved in allergic inflammation
IL15	Interleukin-15	- Secreted by mononuclear phagocytes - Induces cell proliferation of NK cells
IL16	Interleukin-16	- Pleiotropic cytokine that functions as a chemoattractant and a modulator of T cell activation
IL17	Interleukin-17	- Proinflammatory cytokine, acts in synergy with IL1 and TNFα
IL18	Interleukin-18	- Proinflammatory cytokine - Produced by macrophages and other cells
IL1Rα	Interleukin-1 receptor alpha chain	- Secreted by immune and epithelial cells - Natural inhibitor of the pro-inflammatory effect of IL1β
IL2Rα	Interleukin-2 receptor alpha	- Transmembrane protein present on activated T-cells and B-cells

	chain	- Soluble form elevated in T-cell lymphoma/leukemia used for disease monitoring.
Chemokines		
MCP1 = CCL2	Chemokine (C-C motif) ligand 2	- Recruits monocytes, memory T cells, and dendritic cells to the sites of inflammation - Implicated in the pathogenesis of atherosclerosis, CTEPH
MIP1α = CCL3	Chemokine (C-C motif) ligand 3	- Produced by macrophages after stimulation by bacterial endotoxin - Activates granulocytes (neutrophils, eosinophils and basophils) leading to acute neutrophilic inflammation - Induces secretion of IL-1, -6 and TNF-α from fibroblasts and macrophages
MIP1β = CCL4	Chemokine (C-C motif) ligand 4	- Idem than CCL3.
RANTES = CCL5	Chemokine (C-C motif) ligand 5	- Recruits T cells, eosinophils, and basophils, - Plays an active role in recruiting leukocytes into inflammatory sites
MCP3 = CCL7	Chemokine (C-C motif) ligand 7	- Specifically attracts monocytes, and regulates macrophage function
CTACK = CCL27	Chemokine (C-C motif) ligand 27	- Plays a role in T-cell mediated inflammation of the skin - Elicits chemotactic effect by binding to the chemokine receptor CCR10
Eotaxins	Chemokine (C-C motif) ligand 11, 24, 26	- Recruits eosinophils
GROa = CXCL1	Chemokine (C-X-C motif) ligand 1	- Expressed by macrophages, neutrophils and epithelial cells - Has neutrophil chemoattractant activity, is involved in angiogenesis, inflammation

		- Has his action through receptor CXCR2
IL8 = CXCL8	Chemokine (C-X-C motif) ligand 8 = Interleukin-8	- Produced by macrophages and endothelial cells - Has neutrophil chemoattractant activity and potently promotes angiogenesis
MIG = CXCL9	Chemokine (C-X-C motif) ligand 9	- Chemoattractant for T-cells
IP10 = CXCL10	Chemokine (C-X-C motif) ligand 10	- Chemoattraction for monocytes/macrophages, T cells, NK cells, and dendritic cells - Promotes T cell adhesion to endothelial cells - Inhibits bone marrow colony formation and angiogenesis
SDF1a = CXCL12	Chemokine (C-X-C motif) ligand 12	- Has lymphocyte chemoattractant activity - Role in angiogenesis - Associated with risk of coronary disease
Growth factors		
MCSF = CSF1	Macrophage colony-stimulating factor = Colony stimulating factor 1	- Hematopoietic growth factor involved in the proliferation, differentiation, and survival of monocytes, macrophages, and bone marrow progenitor cells - Involved in the development and progression of atherosclerosis
NGF	Nerve growth factor	- Involved in the growth, maintenance, proliferation, and survival of neurons - Role in the regulation of the immune system - Released in high concentrations by mast cells, playing a role in pain perception in areas under inflammation - Released by CD4+ T cell clones, inducing a cascade of maturation of T cells under infection - The expression of NGF is increased in inflammatory diseases such as asthma where it suppresses

		inflammation - Role in cardiovascular disease (reduced levels of NGF in acute coronary syndromes) - Increased in the right ventricle of mice with PH model
SCF	Stem cell factor	- Role in hematopoiesis - Cardiomyocyte-specific overexpression of transmembrane SCF promotes stem cell migration and improves cardiac function and animal survival after myocardial infarction
SCGFβ	Stem cell growth factor beta	- Hematopoietic growth factors
TNFα	Transforming growth factor alpha	- Mainly produced by activated macrophages - Proinflammatory cytokine - Promotes the development of PAH by reducing BMPR2 expression, promoting BMPR-II cleavage in vascular cells, and driving inappropriate proliferation of smooth muscle cells in pulmonary arteries
TNFβ	Transforming growth factor beta 1	- Role in immunoregulation - Negative autocrine growth factor
HGF	Hepatic growth factor	- Paracrine factor normally produced by cells of mesenchymal origin (fibroblasts, macrophages) - Role in normal embryogenesis and development, and in adults, role in tissue repair - Cardioprotective properties reported in the left heart - High circulating associated levels in left pressure overloaded disease and left heart failure
PDGFbb	Platelet-derived growth factor bb	- Role in angiogenesis - Produced by platelets upon activation, smooth

		muscle cells, activated macrophages, and endothelial cells
FGF2 = FGFβ	Basic fibroblast growth factor	- Mitogenic, involved in cell survival activities and angiogenesis
GCSF	Granulocyte colony-stimulating factor	- Stimulates the bone marrow to produce granulocytes and stem cells and release them into the bloodstream - Stimulates the survival, proliferation, differentiation, and function of neutrophils precursors and mature neutrophils
GMCSF	Granulocyte-macrophages colony-stimulating factor	- Secreted by macrophages, T cells, mast cells, natural killer cells, endothelial cells and fibroblasts - Promotes neutrophil, macrophages and eosinophil proliferation and maturation
VEGF-A	Vascular endothelial growth factor-A	- Role in angiogenesis and vasodilation - Chemotactic for granulocytes and macrophages
Other cytokines		
MIF	Macrophage migration inhibitory factor	- Proinflammatory cytokine - Involved in cell-mediated immunity, immunoregulation, and inflammation - In PAH: elevated concentrations of MIF - In mouse models of PH: antagonism of MIF inihibits hypoxia-induced smooth cell proliferation
TRAIL	TNF-related apoptosis-inducing ligand	- Induces apoptosis
IFNA2	Interferon alpha-2	- Potent antitumor activity, activation of the immune system which can eliminate tumor cell
IFNγ	Interferon gamma	- Important role for innate and adaptive immunity against viral, bacterial and protozoal infections - Activator of macrophages and MHC II

Table E2. Right heart risk scores. Mayo Clinic derived-score and Stanford-derived score for prediction of death, lung transplant or admission at 3 years in the recently published Vera Moulton Wall Center cohort (3).

Mayo Clinic score		**Stanford score**	
Variables	Points	Variables	Points
RV longitudinal strain (%)		RV end-systolic remodeling index	
≥25 (reference)	0	<1.32 (reference)	0
[20 – 25[	3	[1.32 - 1.45[	2
[15 – 20[	5	[1.45 - 1.60[	3
<15	5	≥1.60	5
NT-proBNP (pg/mL)		NT-proBNP (pg/mL)	
< 1500	0	< 1500	0
≥ 1500	1	≥ 1500	2
NYHA class		NYHA class	
I or II	0	I or II	0
III or IV	3	III or IV	3
Total	/17	Total	/15

NYHA: New York Heart Association; RV: right ventricular.

Table E3. REVEAL PAH Risk Score. *Adapted from Benza et al. Circulation, 2010.*

Variables	
WHO Group I Subgroup	APAH-Connective Tissue Disease: +1 APAH-Portal Hypertension: +2 Familial-PAH: +2
Demographics and Comorbidities	Renal Insufficiency: +1 Males Age > 60years: +2
NYHA/WHO Functional Class	I: -2 III: +1 IV: +2
Vital Signs	Systolic Blood Pressure <110mmHg: +1 Heart Rate > 92bpm
6-Minute Walk Test	> or = 440m: -1 < 165m: +1
BNP levels	< 50pg/mL: -2 > 180 pg/mL: +1
Echocardiogram	Pericardial Effusion: +1
Pulmonary Function Test	% predicted DLCO > or =80: -1 % predicted DLCO < or =32: +1
Right Heart Catheterization	Mean Right Atrial Pressure > or =20mmHg within 1 year: +1 Pulmonary Vascular Resistance >32 Wood units: +2

Table E4. Characteristics of the patients with pulmonary arterial hypertension (PAH) from which right ventricular biopsies were obtained.

	Age (years)	**Sex**	**PH etiology**	**NYHA class**	**MPAP (mmHg)**	**Preoperative PH-specific therapy**
Patient 1	43	Male	Eisenmenger (Atrial Septal Defect)	III	51	PDE5I, ERB, treprostinil
Patient 2	24	Female	Drug and Toxin	III	50	PDE5I, ERB, prostacyclin
Patient 3	61	Female	Idiopathic	IV	59	PDE5I, ERB, treprostinil
Patient 4	52	Female	BMPR2 mutation	III	64	PDE5I, ERB, prostacyclin

ERB: endothelin receptor blocker; MPAP: mean pulmonary arterial pressure; NYHA: New York Heart Association functional class; PDE5I: phosphodiesterase inhibitor; PH: pulmonary hypertension.

Table E5. Biomarkers with significant partial least square regression coefficients for association with right heart metrics.

	High cytokine level associated with "unfavorable" metric		**High cytokine level associated with "favorable" metric**	
	Discovery	Validation	Discovery	Validation
Mayo right heart score	**SCGF**β **HGF** **NGF** MCSF SDF1a MIG	**HGF** **SCGF**β **NGF**	TRAIL IL2Rα	None
Stanford right heart score	**SCGF**β **HGF** **NGF** SDF1a Eotaxin	**SCGF**β **HGF** **NGF** VEGF	None	None
RVLS	**SCGF**β **HGF** SDF1a **NGF**	**HGF** **SCGF**β **NGF**	PDGFβ GMCSF TNFα	None
RVESRI	**HGF** **SCGF**β **NGF**	**SCGF**β **HGF**	PDGFβ IL3 GCSF	None

	MCP1			
	Eotaxin			
NT-proBNP (log)	**HGF**	**HGF**	TRAIL	None
	SCGFβ		ILR2α	
	NGF		PDGFβ	
	MIG		LIF	
	SDF1a		IL3	
			MCP3	
NYHA class	**HGF**	None	None	None
	SCGFβ			
	MIG			
	MCSF			
MPAP	None	None	MCP3	None
PVR	None	None	SCF	SCF
				IL12

P values <0.05 using Jacknife test were considered significant. MPAP: mean pulmonary arterial pressure; PVR: pulmonary vascular resistance; NT-proBNP: N-terminal pro-b type natriuretic peptide; NYHA: New York Heart Association; RVESRI: right ventricular end-systolic remodeling index; RVLS: right ventricular free-wall longitudinal strain. For circulating biomarkers abbreviations, please see **Table E1**.

Table E6. Multivariable Cox regression analysis models for prediction of the primary end point (death, transplant or readmission for heart failure) at 3 years in the total PAH cohort (n=197).

Variables were entered in the model using enter mode. The Mayo right heart score was based on the New York Heart Association class, NT-proBNP and right ventricular longitudinal strain (RVLS). The Stanford right heart score was based on the New York Heart Association class, NT-proBNP and right ventricular end-systolic remodeling index (RVESRI). The REVEAL score was based on the Registry to Evaluate Early And Long-term PAH Disease Management (REVEAL) groups: low, average, moderate high, high, very high. HGF: hepatic growth factor; NGF: nerve growth factor; SCGFβ: stem cell growth factor beta and SDF1: stromal cell-derived factor 1.

	Unadjusted Hazard ratio	95% confidence interval	p value	$\chi 2$	-2Log Likelihood	p value
REVEAL score-based models						
Model 1				46.47	357.77	<0.0001
REVEAL score	1.52	1.33; 1.73	<0.0001			
Model 2				52.96	353.20	<0.0001
REVEAL score	1.45	1.26; 1.67	<0.0001			
HGF	1.01	1.01; 1.02	0.03			
Model 3				50.80	354.10	<0.0001
REVEAL score	1.57	1.37; 1.79	<0.0001			
NGF	0.99	0.99; 1.01	0.07			
Model 4				47.22	357.41	<0.0001
REVEAL score	1.53	1.34; 1.76	<0.0001			
SCGFβ	0.99	0.99; 1.00	0.56			

Model 5				44.69	356.88	<0.0001
REVEAL score	1.54	1.35; 1.76	<0.0001			
SDF1	0.99	0.99; 1.00	0.36			
Stanford score-based models						
Model 1				34.00	370.78	<0.0001
Stanford score	1.36	1.22; 1.52	<0.0001			
Model 2				45.50	364.13	<0.0001
Stanford score	1.28	1.14; 1.45	<0.0001			
HGF	1.01	1.01; 1.02	<0.01			
Model 3				35.63	369.31	<0.0001
Stanford score	1.38	1.23; 1.55	<0.0001			
NGF	0.99	0.99; 1.00	0.25			
Model 4				34.28	369.98	<0.0001
Stanford score	1.40	1.23; 1.58	<0.0001			
SCGFβ	0.99	0.99; 1.00	0.39			
Model 5				34.11	370.68	<0.0001
Stanford score	1.37	1.22; 1.53	<0.0001			
SDF1	1.00	0.99; 1.00	0.36			
Mayo score-based models						
Model 1				27.69	373.05	<0.0001
Mayo score	1.67	1.35; 2.07	<0.0001			
Model 2				43.31	363.23	<0.0001
Mayo score	1.53	1.24; 1.88	<0.0001			
HGF	1.01	1.00; 1.01	0.001			
Model 3				28.36	371.83	<0.0001
Mayo score	1.72	1.38; 2.15	<0.0001			
NGF	0.99	0.99; 1.00	0.29			

Model 4				27.79	373.05	<0.0001
Mayo score	1.67	1.34; 2.09	<0.0001			
SCGFβ	1.00	0.99; 1.00	0.97			
Model 5				27.69	373.01	<0.0001
Mayo score	1.68	1.35; 2.08	<0.0001			
SDF1	1.00	0.99; 1.00	0.83			

References

1. Amsallem M, Sweatt AJ, Aymami MC, Kuznetsova T, Selej M, Lu H, Mercier O, Fadel E, Schnittger I, McConnell MV, Rabinovitch M, Zamanian RT, Haddad F. Right Heart End-Systolic Remodeling Index Strongly Predicts Outcomes in Pulmonary Arterial Hypertension: Comparison With Validated Models. Circ Cardiovasc Imaging 2017; 10.
2. Boehm M, Tian X, Mao Y, Ichimura K, Dufva MJ, Ali K, Prosseda SD, Shi Y, Kuramoto K, Reddy S, Kheyfets VO, Metzger RJ, Spiekerkoetter E. Delineating the molecular and histological events that govern right ventricular recovery using a novel mouse model of PA de-banding. Cardiovasc Res 2019;doi:10.1093/cvr/cvz310.
3. Mevik BH and Wehrens R. The pls package: Principal component and partial least squares regression in R. Journal of Statistical Software, 18:1–24, 2007.
4. Mevik BH and Cederkvist HR. Mean squared error of prediction (MSEP) estimates for principal component regression (PCR) and partial least squares regression (PLSR). Journal of Chemometrics, 18:422–429, 2004.